JACS
JOURNAL OF THE AMERICAN CHEMICAL SOCIETY
Article
pubs.acs.org/JACS

Electronic Structure of Ni_2E_2 Complexes (E = S, Se, Te) and a Global Analysis of M_2E_2 Compounds: A Case for Quantized E_2^{n-} Oxidation Levels with n = 2, 3, or 4

Shu A. Yao,[†] Vlad Martin-Diaconescu,[‡] Ivan Infante,[§] Kyle M. Lancaster,[∥] Andreas W. Götz,[⊥] Serena DeBeer,[‡,∥] and John F. Berry*[,†]

[†]Department of Chemistry, University of Wisconsin—Madison, 1101 University Avenue, Madison, Wisconsin 53706, United States
[‡]Max Planck Institute for Chemical Energy Conversion, Stiftstrasse 34-36, D-45470, Mülheim/Ruhr, Germany
[§]Kimika Fakultatea, Euskal Herriko Unibertsitatea, and Donostia International Physics Center (DIPC), P. K. 1072, 20080 Donostia, Euskadi, Spain
[∥]Department of Chemistry and Chemical Biology, Cornell University, Ithaca, New York 14853, United States
[⊥]San Diego Supercomputer Center, University of California—San Diego, La Jolla, California 92093, United States

Supporting Information

ABSTRACT: The diamagnetic compounds $Cp'_2Ni_2E_2$ (**1**: E = S, **2**: E = Se, **3**: E = Te; Cp′ = 1,2,3,4,-tetraisopropylcyclopentadienyl), first reported by Sitzmann and co-workers in 2001 [Sitzmann, H.; Saurenz, D.; Wolmershauser, G.; Klein, A.; Boese, R. *Organometallics* **2001**, 20, 700], have unusual E···E distances, leading to ambiguities in how to best describe their electronic structure. Three limiting possibilities are considered: case **A**, in which the compounds contain singly bonded E_2^{2-} units; case **B**, in which a three-electron E.∴E half-bond exists in a formal E_2^{3-} unit; case **C**, in which two E^{2-} ions exist with no formal E−E bond. One-electron reduction of **1** and **2** yields the new compounds $[Cp^*_2Co][Cp'_2Ni_2E_2]$ (**1red**: E = S, **2red**: E = Se; Cp* = 1,2,3,4,5-pentamethylcyclopentadieyl). Evidence from X-ray crystallography, X-ray absorption spectroscopy, and X-ray photoelectron spectroscopy suggest that reduction of **1** and **2** is Ni-centered. Density functional theory (DFT) and ab initio multireference methods (CASSCF) have been used to investigate the electronic structures of **1**−**3** and indicate covalent bonding of an E_2^{3-} ligand with a mixed-valent Ni_2(II,III) species. Thus, reduction of **1** and **2** yields Ni_2(II,II) species **1red** and **2red** that bear unchanged E_2^{3-} ligands. We provide strong computational and experimental evidence, including results from a large survey of data from the Cambridge Structural Database, indicating that M_2E_2 compounds occur in quantized E_2 oxidation states of $(2 \times E^{2-})$, E_2^{3-}, and E_2^{2-}, rather than displaying a continuum of variable E−E bonding interactions.

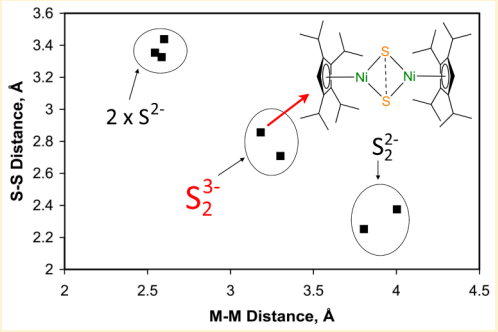

INTRODUCTION

The chalcogens are versatile elements with a broad range of available oxidation states ranging from +6 to −2. Metal-mediated redox processes of the chalcogens are vital in biological systems,[1] industrial catalysis,[2] and organic electronics,[3] as well as in nanomaterials[2m,4] and semiconductor fabrication.[1g,2n,o,3b,d,4e,5] Chalcogen−chalcogen bond formation and cleavage are two of the most fundamental of these processes. Unlike the corresponding oxygen compounds, those that contain a singly bonded E−E unit with E = S, Se, or Te can undergo stepwise, reversible, single-electron transfer reactions (Scheme 1A) that cleave the E−E bond via E.∴E intermediates having a three-electron (3e) E−E σ half-bond,[6] which is isovalent to He_2^+, as depicted in Scheme 1B,C. Several examples of E.∴E 3e half-bonded radical cations have been isolated, stabilized by bridging organic ligands,[7] such as the recently reported naphthalene derivatives shown in Scheme 1D.[7c,d] In principle, the simplest examples of 3e-bonded E.∴E species are the E_2^{3-} ions, or "subchalcogenide" ions, highlighted in Scheme 1A,C, which remain unknown. However, it has recently been suggested that the E_2^{3-} ions could be stabilized as ligands to metal centers.[8]

A pair of chalcogen atoms may bind to transition metals in several different oxidation states. Singly bonded dichalcogenide E_2^{2-} (E = S, Se, and Te) ligands have a two-electron single bond between two E atoms and can bind as a ligand in multiple coordination modes. E−E single bond distances of 2.04, 2.32, and 2.72 Å are expected for E = S, Se, and Te, respectively, based on the single-bond covalent radii reported by Pyykkö and co-workers.[9] Alternatively, two nonbonded E^{2-} ligands can bridge two metal atoms to make a M_2E_2 diamond-shaped unit in which the E···E distance will approach the sum of the van der Waals radii (3.78 Å for S_2, 3.64 for Se_2, and 3.98 for Te_2).[10]

Received: November 11, 2014
Published: March 21, 2015

DOI: 10.1021/ja511607j
J. Am. Chem. Soc. 2015, 137, 4993−5011

Scheme 1. A, One-Electron Redox Processes of Dichalcogen Species. B. Electronic Structure of the $[He_2]^+$ Cation Highlighting the $\sigma^2\sigma^{*1}$ Three-Electron Half-Bond. C. Electronic Structure of the $[E_2]^{3-}$ Ions Highlighting the Three-Electron Half σ Bond. D. A Recent Example of Three-Electron Half-Bonded E_2 Species Supported by Organic Ligands. E. The Compounds Studied in This Paper

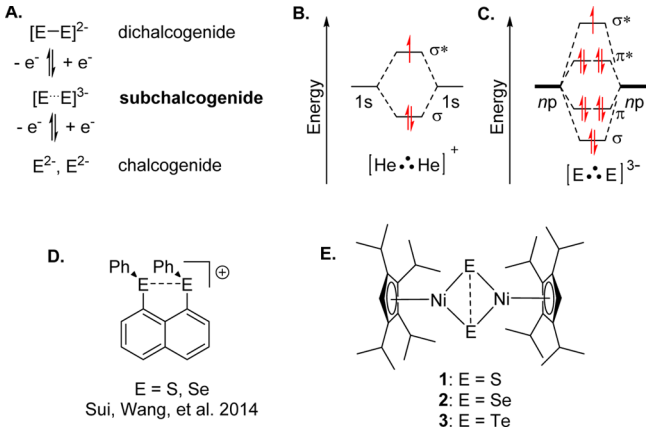

Odd-electron E_2 species are rare. The S_2^- ligand, termed "supersulfide" as an analogue to the well-known superoxide, has been identified in a number of transition metal complexes,[11,12] and has been suggested for uranium compounds.[13] The heavier analogues Se_2^- and Te_2^- have been proposed to exist in complexes that are unstable with respect to dimerization.[14] Recently, "subsulfide" S_2^{3-}[8] and "subselenide" Se_2^{3-} ions[15] have been proposed by us as ligands to transition metals; these species represent new additions to the family of E_2^{n-} compounds with n = 0, −1, −2, and now −3.

The subsulfide proposal has, in particular, been controversial. A S_2^{3-} ligand was originally proposed to explain the unusual triplet ground state of the $[Cu_3S_2(tmeda)_3]^{3+}$ ion (tmeda = tetramethylethylenediamine),[11c,16] for which experimental data are inconsistent with either a S_2^{2-} or a 2 × S^{2-} assignment.[17] The presence of a S_2^{3-} ligand in this complex was suggested[8] based on density functional theory (DFT) calculations utilizing the corresponding orbital transformation,[18] which indicate strong spin pairing between three Cu(II) ions and a S_2^{3-} ligand.[8] Data from Cu K-edge XAS measurements are consistent with the Cu(II) assignment (which, from charge balance considerations would indicate a S_2^{3-} ligand), but S K-edge X-ray absorption spectroscopy (XAS) data were interpreted as indicating an oxidation state for S between −1.5 and −2.0.[19] Subsequent computational studies on the Cu_3S_2 compound from two other research groups further support the subsulfide assignment.[20] Recently, Kaupp, Driess, and co-workers developed a heterobimetallic approach to target the deliberate preparation of compounds containing the S_2^{3-} ion and characterized a $[NiS_2Pt]$ complex described as having ~40% S_2^{3-} character on the basis of the calculated spin density on S.[21]

Concurrent with the above investigations, we have taken a cue from a histogram of reported S···S distances from the Cambridge Structural Database (CSD) that was compiled by Alvarez[10] and noticed the existence of a number of compounds having S···S separations that could represent extant examples of subsulfido complexes. In this way, our attention was drawn to a remarkable series of organometallic compounds reported by Sitzmann and co-workers in 2001 with the general formula $Cp'_2Ni_2E_2$ (**1**−**3**, Scheme 1), with Cp′ = tetraisopropylcyclopentadienyl, and E = S, Se, and Te.[22] The properties of these compounds (crystal structures, electrochemical data, and UV−vis spectra) were described by Sitzmann et al. as being inconsistent with either an E_2^{2-} formulation or a 2 × E^{2-} formulation. We therefore wondered whether this series of compounds could possibly contain the entire family of subchalcogenide ions and embarked on an extensive experimental/computational study of their electronic structures. While Sitzmann and co-workers determined the X-ray crystal structures of **1**−**3**, the reported room temperature crystallographic data resulted in significant disorder of the positions of the chalcogen atoms. We report here the results of high-quality, low temperature X-ray crystal structure determinations of **1**−**3**, as well as key experiments aimed to probe the physical oxidation states of the metal and chalcogen atoms in the compounds: X-ray absorption spectroscopy and X-ray photoelectron spectroscopy. These results, coupled with high-level computational studies utilizing DFT, as well as complementary ab initio multireference methods, provide a clear view of the bonding in these compounds. Additionally, we report the results of chemical reduction of compounds **1** and **2**; results on the Se congener **2** have been previously communicated.[15]

RESULTS AND DISCUSSION

Synthesis. The known compounds **1**− **3** were prepared according to the protocols reported by Sitzmann and co-workers, [22] via the reaction of $Cp'_2Ni_2Br_2$ with the Na_2E_2 salts. The reported[22a] electrochemical data of **1** and **2** indicated that both compounds could undergo one-electron reduction, which was achieved as described in Scheme 2. Compounds **1** and **2**

Scheme 2. (a) Synthesis of 1−3 from $Cp'_2Ni_2Br_2$ by Reaction with Na_2E_2 as Described in Ref 22a. (b) Chemical Synthesis of 1red and 2red by One Electron Reduction of 1 and 2 by Reaction with Cp^*_2Co

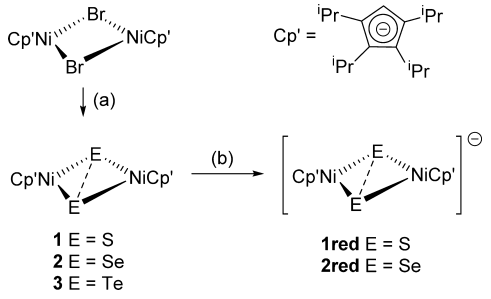

react readily with Cp^*_2Co (Cp^* = 1,2,3,4,5-pentamethylcyclopentadieyl) to produce the corresponding salts containing the new one-electron reduced monoanions: $[Cp^*_2Co]^+[Cp'_2Ni_2S_2]^-$ (**1red**) and $[Cp^*_2Co]^+[Cp'_2Ni_2Se_2]^-$ (**2red**). The nickelocenium analogue $[Cp'_2Ni]^+BF_4^-$ (**4**) was isolated by oxidation of **1** at room temperature.

X-ray Crystal Structures. Low-temperature (100 K) crystal structures of the known compounds **1**− **3** and all the new compounds have been obtained. The crystallographic data for all compounds are given in Table 1. The crystal structures of **1** and **2** both belong to the space group $C2/c$, in which the Ni_2E_2 core is located on a crystallographic inversion center (i.e., Z = 4; **1** in Figure 1 and **2** in Figure S1, Supporting Information). In the unit cell of **3** $(Cp'NiTe)_2$, there are five dimeric molecules (triclinic space group $P\bar{1}$), with two pairs of

DOI: 10.1021/ja511607j
J. Am. Chem. Soc. 2015, 137, 4993−5011

Table 1. Crystal Data for 1, 1red, 2, 2red, 3, and 4

	1	1red	2	2red	3	4
formula	$C_{34}H_{58}Ni_2S_2$	$C_{54}H_{88}Ni_2S_2Co$	$C_{34}H_{58}Ni_2Se_2$	$C_{54}H_{88}Ni_2Se_2Co$	$C_{34}H_{58}Ni_2Te_2$	$C_{34}H_{58}NiBF_4$
formula weight, g/mol	742.16	977.71	742.16	1071.51	839.42	612.32
crystal system	monoclinic	monoclinic	monoclinic	monoclinic	triclinic	orthorhombic
space group	$C2/c$	$P2_1/c$	$C2/c$	$P2_1/c$	$P\bar{1}$	$Pbca$
a, Å	18.55(2)	20.995(4)	18.55(2)	21.2558(5)	12.551(1)	16.228(1)
b, Å	17.68(2)	11.757(2)	17.68(2)	11.8529(3)	18.043(1)	18.979(1)
c, Å	11.62(1)	21.175(4)	11.62(1)	21.0283(5)	20.207(1)	21.505(1)
α, deg	90	90	90,	90	72.35(1)	90
β, deg	115.38(1)	99.84(3)	115.38(1)	100.397(1)	89.89(1)	90
γ, deg	90	90	90	90	84.42(1)	90
V, Å^3	3442(6)	5150(2)	3442(6)	5210.9(2)	4341.4(6)	6623.6(4)
Z	4	4	4	4	5	8
ρ, mg m^{-3}	1.432	1.261	1.432	1.367	1.603	1.228
R1[a], wR2[b] ($I < 2\sigma(I)$)	0.0292, 0.1148	0.0280, 0.0642	0.0292, 0.1148	0.0196, 0.0827	0.0383, 0.0721	0.0435, 0.0886
R1[a], wR2[b] (all data)	0.0350, 0.1223	0.0404, 0.0697	0.0350, 0.1223	0.0236, 0.0894	0.0640, 0.0781	0.0839, 0.1019

[a] $R1 = \sum||F_o| - |F_c||/\sum|F_o|$. [b] $wR2 = [\sum[w(F_o^2 - F_c^2)^2]/\sum[w(F_o^2)^2]]^{1/2}$, $w = 1/\sigma^2(F_o^2) + (aP)^2 + bP$, where $P = [\max(0 \text{ or } F_o^2) + 2(F_c^2)]/3$.

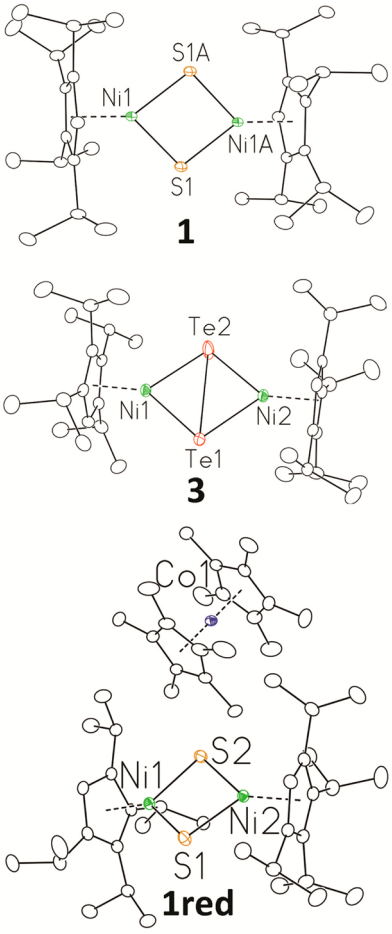

Figure 1. Crystal structures of **1** $(Cp'NiS)_2$ (Cp′ = 1,2,3,4-tetraisopropylcyclopentadienyl), **3** $(Cp'NiTe)_2$ and **1red** $[Cp^*_2Co]^+[(Cp'NiS)_2]^-$. The relevant bond distances and angles are listed in Supporting Information. All molecules are drawn with displacement ellipsoids at 30% probability, and all hydrogen atoms have been omitted for clarity. Relevant bond distances and angles are listed in Table 1

dimers located on general positions, with the fifth molecule located on a crystallographic inversion center (Figure 1). All relevant bond distances and angles are listed in Table 2. For each structure, the Ni_2E_2 core is diamond-shaped, with all four atoms in the same plane, and is situated between two parallel five-membered cyclopentadienyl rings. The Ni···Ni distances of 3.225(1) Å in **1**, 3.438(3) Å in **2**, and 3.788(2) Å in **3** are all too long to consider any Ni−Ni bonding interaction. The E···E distances of 2.806(1) Å in **1** (E = S), 2.915(3) Å in **2** (E = Se), and 3.115(3) Å in **3** (E = Te) are all intermediate between E−E single-bond distances and the sum of van der Waals radii of two E atoms (vide infra). The reduced species $[Cp^*_2Co]^+[(Cp'NiS)_2]^-$ (**1red**, see Figure 1) and $[Cp^*_2Co]^+[(Cp'NiSe)_2]^-$ (**2red**) retain the overall structure of the Ni_2E_2 diamond core, but both structures show a fairly close association of the $[Cp^*_2Co]^+$ cation with the anionic $[Cp'_2Ni_2E_2]^-$ unit.

Complexes **1red** $[Cp^*_2Co]^+[(Cp'NiS)_2]^-$ and **2red** $[Cp^*_2Co]^+[(Cp'NiSe)_2]^-$ have almost identical crystal structures in the space group $C2/c$. The reduced complex anion $[(Cp'NiS)_2]^-$ is very similar in geometry to the neutral complex, with a minor elongation by 0.034(2) Å of the S···S distance, while the separations between the two Ni atoms remain the same (3.225(1) Å in **1red** versus 3.224(1) Å in **1**). It is worth mentioning that the Ni_2S_2 core is not planar but is slightly bent along the S···S vector, such that the angle between the Ni(1)S_2 plane and the Ni(2)S_2 plane is 166.4°. The closest C atom on the Cp* ring in the countercation $[Cp^*_2Co]^+$ lies 3.76 Å away from the isopropyl C atom in the anionic $[(Cp'NiS)_2]^-$ moeity. This relatively close nonbonded contact in **1red** is likely the cause for the slight bend along the S···S vector. The distance between the Ni and the Cp′ plane is significantly elongated by 0.045(2) Å upon one-electron reduction, suggesting that the reduction is Ni-centered. This view is further supported by the elongation of the Ni−S distances by 0.021 Å upon reduction. The geometry of **2red** $[Cp^*_2Co]^+[(Cp'NiSe)_2]^-$ can be described in the same manner as that of **1red**. Elongation of the Ni−Cp' centroid distance by 0.023 Å and the Ni−Se distances by 0.019 Å point to a Ni-centered reduction process. The Se···Se distance is elongated by 0.077 Å.

Limiting Resonance Structures of 1− 3. On the basis of their crystal structures, we may consider three limiting cases for the electronic structures of **1**−**3**, outlined in Scheme 3, depending on how we assign the nature of the E···E interaction.

DOI: 10.1021/ja511607j
J. Am. Chem. Soc. 2015, 137, 4993−5011

Table 2. Summary of Distances and Angles for Complexes 1, 1red, 2, 2red, 3, and 4

	E−E (Å)	Ni−E (Å)	Ni···Ni (Å)	Ni−Cp′[a] (Å)	E−Ni−E (deg)	Ni−E−Ni (deg)	Ni−E−E−Ni (deg)
1 $(Cp'NiS)_2$	2.806(1)	2.137[1]	3.225(1)	1.725(2)	82.04(2)	97.96(2)	180(1)
$\mathbf{1}_{red}$ $[Cp^*_2Co](Cp'NiS)_2$	2.841(2)	2.158[2]	3.226(1)	1.770[2]	82.32[6]	96.75[7]	166.42(6)
2 $(Cp'NiSe)_2$	2.915(3)	2.254[2]	3.438(3)	1.728(2)	80.60(1)	99.40(1)	180(1)
$\mathbf{2}_{red}$ $[Cp^*_2Co](Cp'NiSe)_2$	2.992(3)	2.273[1]	3.400(1)	1.751[2]	82.32[1]	96.81[1]	166.80(1)
3 $(Cp'NiTe)_2$	3.115(3)	2.440[2]	3.771(3)	1.736[2]	79.86 (2)	100.44(2)	180(1)
4 $[Cp'_2Ni]BF_4$	N/A	N/A	N/A	1.784[2]	N/A	N/A	N/A

[a]The distance between Ni and the Cp′ centroid.

Scheme 3. Limiting Resonance Forms for 1−3

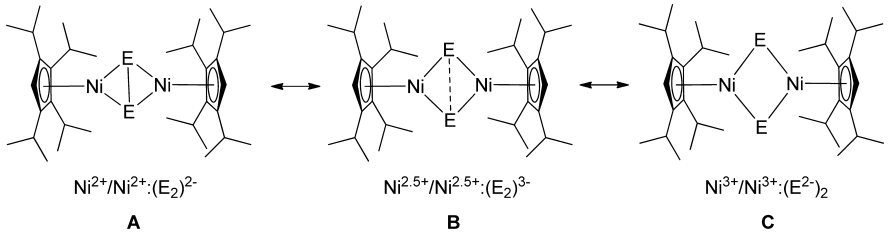

If we assume an E−E single bond, then this implies an E_2^{2-} ligand, necessitating an assignment of 2+ for the oxidation state of each Ni atom (case **A**). For an E.˙.E 3e half-bond, the E_2^{3-} ligand requires Ni mixed-valency, either localized (i.e., Ni(II)/Ni(III)) or delocalized with an overall average nonintegral Ni oxidation state of 2.5+ (case **B**). If we assume that the structure does not contain any E−E bond, then the chalcogens must be assigned as nonbonded E^{2-} ligands, with both Ni ions in the 3+ oxidation state (case **C**). Cases **A**−**C** are formally one-electron resonance structures of one another; they have the same valence electron count. All three of these structures may contribute to the bonding in the compound. We use the evidence collected here to decide which one(s) provide the most accurate description of the electronic structures and redox reactivity of the compounds.

Cases **A**−**C** are all consistent with the observed diamagnetism of **1**−**3** (vide infra). In particular, **A** may be considered to be the most likely case to display paramagnetism, since the known Ni(II)/Ni(II) compounds bearing Br or Cl ligands are in fact paramagnetic at room temperature.[22b] Moreover, the hydride complex $(Cp'NiH)_2$ has a spin-triplet ground state.[23] Nevertheless, it is possible for a CpNi unit to exist in either a high-spin (S = 1) or low-spin (S = 0) form. With this in mind, case **B** may also be expected to be diamagnetic. In the localized limit, a high-spin Ni(II) (S = 1) can pair with the two unpaired spins of the S_2^{3-} and Ni(III) to give a diamagnetic ground state. In the case of a low-spin Ni(II), we need only invoke pairing of the S_2^{3-} spin with that of the Ni(III). For a fully delocalized Ni(2.5+) mixed-valent species, the $(Ni_2)^{5+}$ unit would together be expected to share a single unpaired electron, which can then pair with the unpaired spin of the S_2^{3-} ligand giving a diamagnetic species. For case **C**, a diamagnetic ground state requires strong spin pairing between two S = 1/2 Ni(III) centers through the sulfide bridges. The Ni−E−Ni angles of >90° in **1**−**3** would allow for antiferromagnetic coupling.

The crystallographic data for **1**−**3** clearly indicate E···E distances between what would be expected for case **A** or case **C**. Indeed, this observation is the origin of our hypothesis that **1**−**3** may best be described as containing E_2^{3-} ligands as in case **B**.

Reduction of **1**−**3** can add an electron either to the E_2 unit or to the metal atoms. Reduction of the E_2 unit is expected to be accompanied by large structural variations in the E···E distance by ≥0.5 Å. However, in the case of Ni-centered redox chemistry, we would not expect to find much change in either the E···E distance for the oxidized or reduced species or in the distance between two nonbonding Ni atoms. One-electron oxidation of **2** was reported[15] to yield a compound with a Se−Se distance, 2.36 Å, drastically shorter than in the neutral compound, which is fully consistent with the formation of a Se_2^{2-} species.[24]

Upon one-electron reduction of **1** and **2**, the geometric changes outlined above indicate an Ni-centered redox process. These data taken together are highly suggestive of case **B** for the electronic structures of **1**−**3**. It should be further noted, however, that the similarity of each Ni site in all of the crystal structures for **1**−**3** would indicate that if case **B** represents the actual electron configuration, then the compounds must be mixed-valent at the fully delocalized (class III) limit. This statement applies to both the Ni mixed valency *and* the S mixed valency. Cases **A**−**C** will be referred to in the discussion below involving other pertinent physical data for these compounds.

NMR Spectroscopy, UV−vis−NIR Absorption Spectroscopy, and Electron Paramagnetic Resonance Spectroscopy. Besides X-ray crystallography, the identities of **1**, **2**, and **3** were also established by ^{1}H NMR spectroscopy, elemental analysis, UV−vis-NIR spectroscopy, and mass spectrometry.[22] As mentioned above, **1**, **2**, and **3** are all diamagnetic, unlike their paramagnetic precursor $(Cp'NiBr)_2$.[22b] Compound **2** was investigated in solution by ^{77}Se NMR spectroscopy. The single sharp peak at 880 ppm indicates chemical equivalence of the two Se atoms in solution, consistent with the solid-state structure. Transition metal complexes bearing the Se_2^{2-} ion show ^{77}Se NMR resonances at <−250 ppm,[25] whereas resonances for Se^{2-} species have appeared as disparately as −996 ppm or +1241 ppm.[25a,26] Therefore, the Se NMR data disfavor a Se_2^{2-} assignment, ruling out case **A**. The ^{125}Te NMR spectrum of **3** displays a single sharp peak at 822 ppm, which also suggests that the two Te atoms are equivalent in solution as in solid state. ^{125}Te NMR resonances for Te^{2-} species in other complexes are known to occur anywhere from −972 ppm to 1124 ppm and can be affected by subtle structural changes.[27] Thus, no definitive

DOI: 10.1021/ja511607j
J. Am. Chem. Soc. 2015, 137, 4993−5011

bonding information can be inferred from the ^{125}Te NMR spectrum of **3**.[27a,b] There are no reported spectra of Te_2^{2-} compounds, to our knowledge.

All three compounds **1**, **2**, and **3** have two major charge transfer transitions that blanket the visible region of the spectrum, as shown in Figure 2 (data given in Table 3). The

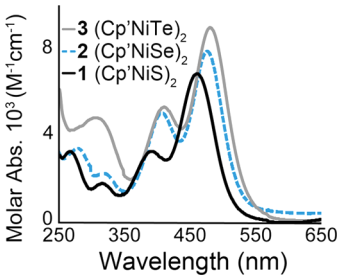

Figure 2. UV−vis absorption spectra of **1** (black), **2** (blue dotted), and **3** (gray) in pentane solution.

Table 3. UV-Vis and Near-IR Absorptions for S, Se, and Te Complexes

	UV−vis absorption (cm^{-1})	near-IR absorption (cm^{-1})	near-IR fwhm (cm^{-1})
1 $[Cp'NiS]_2$	31050 (320 nm, ε = 1790)	14000 (716 nm, ε = 640)	1496
	25200 (394 nm, ε = 3310)	7520 (1329 nm, ε = 93)	
	21500 (464 nm, ε = 6900)		
2 $[Cp'NiSe]_2$	30860 (324 nm, ε = 2230)	13550 (738 nm, ε = 910)	1141
	24940 (401 nm, ε = 5080)	6850 (1460 nm, ε = 190)	
	20880 (479 nm, ε = 7900)		
3 $[Cp'NiTe]_2$	32260 (314 nm, ε = 3700)	11760 (805 nm, ε = 1100)	N/A
	24100 (420 nm, ε = 4900)		
	20620 (487 nm, ε = 6800)		

most intense bands for **2** and **3** appear around 20 800 cm^{-1}, while the band for **1** is slightly blue-shifted, appearing at ~21 550 cm^{-1}. The observed increases in molar absorptivity from S to Te are most likely due to greater orbital overlap as the atomic radii increase since the ratio of observed to theoretical[9] Ni−E bond distances decreases from S (1.003) to Se (0.997) to Te (0.992). Compounds **1**−**3** have electronic spectra that trail into the near-IR region. Low-energy bands at 7520 (fwhm =1496) and 6850 (fwhm =1141) cm^{-1} are observed for **1** and **2**, respectively (See Figures S2 and S3, Supporting Information). The nature of these low-energy bands will be described later.

One-electron reduction of **1** and **2** gives rise to **1red** and **2red**, respectively, each of which features an anionic $[(CpNiE)_2]^-$ unit with a $[Cp^*_2Co]^+$ countercation. Spin states of $S = 1/2$ for **1red** and **2red** are assigned on the basis of the EPR spectra of these compounds (Figure S4, Supporting Information; see ref 15 for the EPR spectrum of **2red**). Both compounds exhibit rhombic EPR spectra in which all three g values are greater than 2. The larger spread in g values for **2red**, as compared to **1red**, is most likely due to the larger spin−orbit coupling contribution for the Se compound, since, as described later, the SOMO has a significant contribution from both the Ni atoms and the chalcogen atoms (vide infra). The g values will be discussed further in the computational section of the paper.

X-ray Absorption Spectroscopy and X-ray Photoelectron Spectroscopy. X-ray absorption spectroscopy (XAS) probes electronic transitions from core orbitals that are highly sensitive to changes in effective nuclear charge and can therefore be useful in assigning a "physical" oxidation state (i.e., an oxidation state based on physical observables) to the elements in a compound. XAS is particularly useful in cases where the oxidation states are ambiguous, as in compounds with redox noninnocent ligands.[15,28] Here, complementary sets of metal and chalcogen XAS data have been collected to aid in assigning the electronic structures of **1**−**3**.

As shown in Figure 3 and Table 4, the S K-edge XAS data of **1** and **1red** each show an intense pre-edge absorption in the

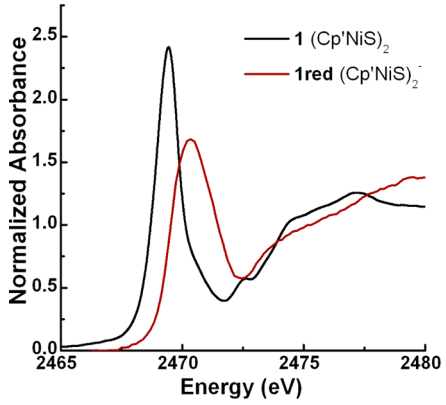

Figure 3. S K-edge XAS spectra of **1** (black) and **1red** (red).

Table 4. Sulfur K-Edge XAS Data, with Energies Extracted As Shown in Figure S11

complex	pre-edge energy (eV)	pre-edge intensity	rising-edge energy
1 $[Cp'NiS]_2$	2469.4	4.26	2473.1
$\mathbf{1}_{red}$ $[Cp'NiS]_2Cp^*Co$	2470.3	3.63	2472.8
$[Cu_3S_2(tmeda)_3]^{3+}$ [a]	2469.5	–	2470.7

[a]Data from ref 19.

2469−2471 eV region, and a broad K-edge around 2473 eV (Figure 3a and Scheme 4). The pre-edge absorption is a transition from the S 1s to unoccupied frontier orbitals within the Ni 3d manifold that have Ni−S antibonding character (vide infra). Similar pre-edge features are observed for transition metal centers with bridging sulfides, disulfides, and thiolates,[29] as well as 3e-bonded perthiyl radicals possessing a singly occupied S 3p orbital.[30] Compound **1** has an intense pre-edge feature at 2469.4 eV with a rising edge visible at ~2473.1 eV. One-electron reduction of **1** yields **1red**, which features a rising edge at 2472.8 eV similar to that in **1**, indicating that the one-electron reduction is not S-based. The pre-edge peak of **1red** shifts to higher energy by ~0.9 eV and decreases in intensity in comparison to that of **1**, consistent with an interaction involving a more reduced Ni center.[29a] As depicted in Scheme 4, the lower Z_{eff} on the Ni will raise the energy of the 3d manifold relative to the S 1s core hole, thus increasing the pre-edge energy. This conclusion is further supported by a decrease

DOI: 10.1021/ja511607j
J. Am. Chem. Soc. 2015, 137, 4993−5011

Scheme 4. Energy-Level Diagram Summarizing the X-ray Spectroscopic Transitions Measured for 1 and 1red[a]

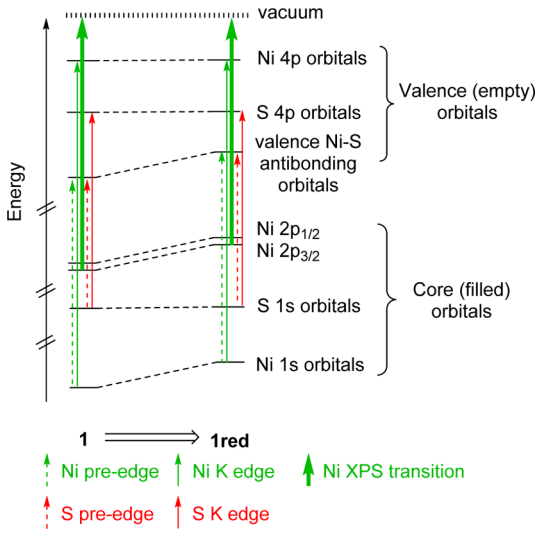

[a]Both core-to-valence (XAS) and core-to-vacuum (XPS) transitions are highlighted, along with the derived changes in orbital positions upon reduction of **1** to **1red**. Occupied orbitals with Ni character are raised in energy upon reduction to **1red** due to the lower Ni Z_{eff}.

in intensity of the **1red** pre-edge feature when compared to **1**, consistent with a loss of "hole" character due to Ni reduction.

The Ni K-edge spectra of **1** $(Cp'NiS)_2$, **2** $(Cp'NiSe)_2$, and **3** $(Cp'NiTe)_2$, shown in Figure 4 and Table 5, are quite similar

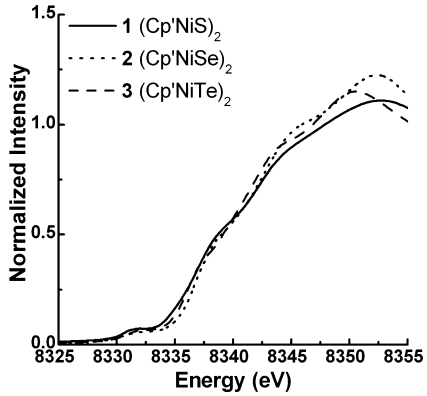

Figure 4. Ni K-edge XAS spectra of **1** (black solid), **2** (black dotted), and **3** (black dash).

Table 5. Nickel K-Edge XAS

	pre-edge energy (eV)	1s → 4p + LMCT (eV)
1 $[Cp'NiS]_2$	8331.4	8338.3
$\mathbf{1}_{red}$ $[Cp'NiS]_2Cp^*Co$	8331.5	8336.6
2 $[Cp'NiSe]_2$	8331.4	8338.2
3 $[Cp'NiTe]_2$	8331.5	8337.7
4 $[Cp'Ni]_2BF_4$	8331.9	–

despite the differences in bridging ligands (S vs Se vs Te). This similarity is a strong indication that all three compounds in the chalcogen series have analogous electronic as well as geometric structures. Looking more closely at the S compounds, the Ni K-edge spectra of **1**, **1red**, and **4** (Ni^{3+} in $[Cp'_2Ni]BF_4$) along with their first derivatives are shown in Figure 5 and Table 5.

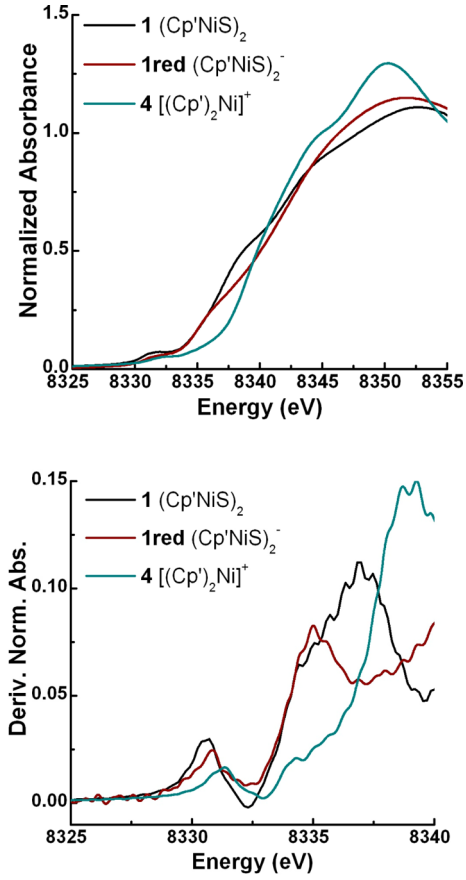

Figure 5. (top) Ni K-edge spectra of **1** (black), **1red** (red), and **4** (dark cyan) and (bottom) the first derivative of Ni K-edge spectra of **1** (black), **1red** (red), and **4** (dark cyan).

Each spectrum contains a band near 8331 eV that corresponds to the 1s → 3d dipole-forbidden transitions. Although the characteristics of this feature are heavily impacted by changes in geometry and ligand environment, the ~0.5 eV higher-energy transition in **4** is nonetheless consistent with its more oxidized Ni(III) center. As reported by Maroney at al., changes in the 1s → 3d pre-edge energy for isoleptic Ni(II)/Ni(III) complementary complexes are small, particularly if sulfur ligands are present. A decrease in intensity for this transition is however to be expected upon reduction.[31] Indeed, this is what we see when comparing the Ni pre-edge transitions of **1** and **1red**: the pre-edge energies are essentially the same, but this feature is less intense in the case of **1red**, suggestive of Ni-centered reduction.

Additionally, higher-energy shoulders to the rising edge are visible, particularly in the derivative spectra, at ~8338.3 eV for **1** and ~8336.6 eV for **1red**, which can be assigned as 1s → 4p + LMCT shake-down transitions. This feature arises from a sulfur-based charge-transfer transition to the Ni and indicates the presence of strongly covalent Ni−S bonds.[31,32] The absence of this band in **4**, which contains no S, provides support for this assignment. The 1s → 4p + LMCT shakedown transition of **1red** is lower in energy by ~1.7 eV than that of **1** and is also lower in intensity. The decrease in the transition energy may be attributed to a Ni-based reduction, and the decrease in the intensity of the shakedown transition indicates decreased Ni−S covalency in **1red**.[33]

A correlation of XAS data with Se physical oxidation states has also been investigated, as shown in Figure S5, Supporting Information. Since no resolved pre-edge features can be

DOI: 10.1021/ja511607j
J. Am. Chem. Soc. 2015, 137, 4993−5011

observed in the Se XAS data, a calibration with the K-edge position was performed by using several Se complexes with known oxidation states ranging from +6 to −1 (Na_2SeO_4, Na_2SeO_3, Se, and Na_2Se_2).[15] A plot of their inflection points, as obtained from the first derivative of the XAS, against oxidation states shows a linear correlation (R_2 = 0.991) that suggests a physical oxidation state of −1.5 for Se in compound **2** directly indicative of a Se_2^{3-} ligand, as in case **B**. We note that a similar calibration with S oxidation states is not appropriate, because of the pre-edge transition to Ni/S admixed molecular orbitals. This feature makes it difficult to accurately define the S K-edge positions[28c,d,34] and underscores the importance of the combined analysis of Ni and S K-edge data above.

X-ray photoelectron spectroscopy (XPS) measures the binding energy of electrons ejected from core orbitals. This technique is widely used to investigate the chemical composition of surfaces,[35] and, like XAS, is also a sensitive tool to probe the physical oxidation states of the elements that make up a sample.[36] Rather than representing transitions to discrete excited states as in XAS, XPS features denote the binding energies of core electrons, which are the energies required to eject them to the vacuum (Scheme 4). Thus, XPS features are less sensitive to the nature of the ligands surrounding a metal center of interest. The XPS data for **1**, **1red**, and **4** in the Ni $2p_{3/2}$ region are shown in Figure 6. The

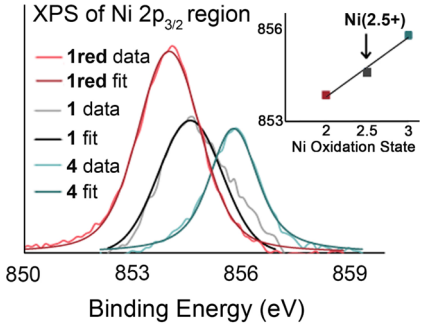

Figure 6. Ni ($2p_{3/2}$) region of XPS spectra of **1** (fit, black; experimental data, light gray), **1red** (fit, red; experimental data, light red), and **4** (fit, dark cyan; experimental, light cyan); inset: plot of the binding energy against the Ni oxidation state.

Ni $2p_{3/2}$ peak is used in this analysis, since it is more intense than the Ni $2p_{1/2}$ signal. In compound **4**, containing the $[Cp'_2Ni]^+$ ion, the Ni oxidation state is unambiguous and may be assigned as Ni^{3+}, in agreement with the binding energy of 856.5 eV, which is the highest binding energy for these three compounds. The binding energy of 855.4 eV for **1** indicates an oxidation state lower than Ni^{3+}, and the binding energy of 853.6 eV for **1red** indicates an oxidation state that is even lower. Thus, we propose that **1** contains fully delocalized (class III mixed-valent) $Ni^{2.5+}$ ions and that **1red** contains Ni^{2+} ions. These data are in agreement with our assignment above that reduction of **1** is Ni-centered rather than S-centered, and that case **B** is the most reasonable assignment for compound **1**. A similar analysis of the XPS data for complexes **2** and **2red** are also consistent with a Ni oxidation state of +2.5 (case **B**) in compound **2** (see Figure S6, Supporting Information).

Vibrational Spectroscopy. The nature of the S···S bonding interaction in **1** was investigated via resonance Raman spectroscopy (Figure 7). Two solid samples, **1** $(Cp'Ni^{32}S)_2$ and ^{34}S-labeled **1iso** $(Cp'Ni^{34}S)_2$, were excited at

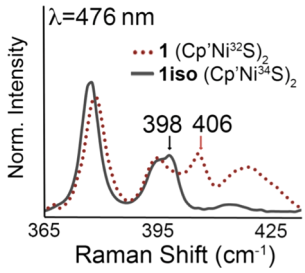

Figure 7. Raman spectra (λ_{ex} = 476 nm) of solid samples of **1** (^{32}S dotted red line) and **1iso** (^{34}S solid black) diluted with KBr.

476 nm at 100 K, and one strongly S-isotope sensitive band at 405.8 cm^{-1} ($\Delta^{34}S_{expl}$ = 7.7 cm^{-1}) was observed. DFT calculations described below suggest that this band is not a S−S stretching vibration. However, in comparison to published ν(S−S) values for singly bonded S_2^{2-} in Na_2S_2 (446 cm^{-1}),[37] one-and-a-half bonded S_2^- (601 cm^{-1}),[38] and doubly bonded S_2 (718 cm^{-1}),[39] the 405.8 cm^{-1} band in **1** is clearly lower in energy. We note that two isotopically sensitive bands in a similar energy region were reported for the $[Cu_3(tmeda)_3S_2]^{3+}$ complex.[16]

Molecular Orbital Considerations. A general molecular orbital picture of the $Cp'_2Ni_2E_2$ compounds may be established in two steps. First, we consider the symmetry-matched orbital interactions that occur between each Ni and its Cp′ ligand. As is well-established from other cyclopentadienyl compounds, the filled Cp′ π orbitals push the Ni $3d_{z^2}$ and $3d_{xz,yz}$ atomic orbitals up in energy, and the unfilled Cp′ π orbitals lower the energies of the Ni $3d_{xy,x^2-y^2}$ orbitals via δ backbonding interactions. Overall, this yields an energy ordering of $d_{xy} \approx d_{x^2-y^2} < d_{z^2} < d_{xz} \approx d_{yz}$ for the Cp′Ni fragment. Under pseudo-D_{2h} symmetry, the pairs of Ni 3d atomic orbitals will transform as follows for their respective in-phase and out-of-phase combinations: $d_{xy} = a_g + b_{1u}$; $d_{x^2-y^2} = b_{1g} + a_u$; $d_{z^2} = a_g + b_{1u}$; $d_{xz} = b_{3u} + b_{2g}$; and $d_{yz} = b_{2u} + b_{3g}$. For reference, the molecular coordinate system is shown at the top of Figure 8.

E−E bonding interactions split the E np orbitals into one σ and two π bonding and antibonding sets. The E−E vector is along the y coordinate. Thus, the p_y−p_y sigma bonding

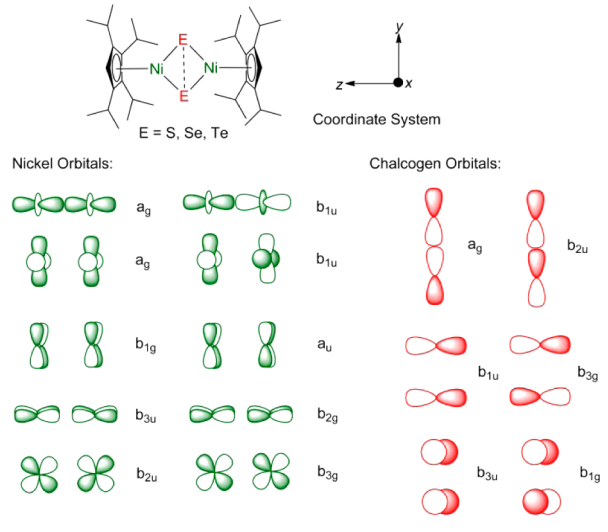

Figure 8. (Top) Molecular coordinate system, and (bottom) symmetry-adapted Ni_2 (green) and E_2 (red) orbital combinations.

DOI: 10.1021/ja511607j
J. Am. Chem. Soc. 2015, 137, 4993−5011

combination transforms as a_g under D_{2h} symmetry, and the corresponding antibonding combination transforms as b_{2u}. The p_z-p_z π and π^* orbitals have b_{1u} and b_{3g} symmetry, respectively, and the corresponding p_x-p_x π and π^* orbitals are b_{3u} and b_{1g}. All of these simple Ni_2 and E_2 orbital combinations are shown in Figure 8.

The relative energies of the Cp′Ni 3d orbitals and the E_2 np orbitals, estimated based on the DFT results, are given at either side of Figure 9. Notably, the E_2 orbitals are fairly closely

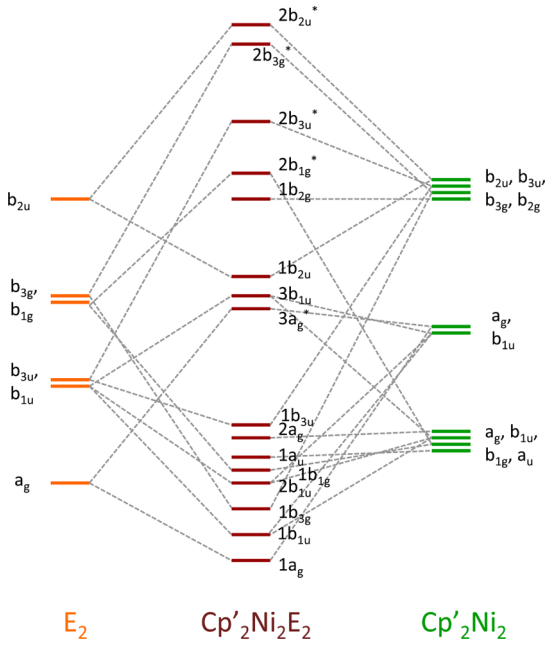

Figure 9. Molecular orbital diagram showing the interactions of the E_2 symmetry-adapted combinations (left) with the Cp'_2Ni_2 combinations. Symmetry labels correspond to the D_{2h} point group and the coordinate system given in Figure 9.

matched in energy with the Cp′Ni orbitals, which, as we shall see, leads to significantly covalent Ni−E interactions. All of the E_2 orbital combinations have appropriate symmetry and energy to interact with Cp′Ni orbitals. The E_2 sigma bonding orbital of a_g symmetry has lobes pointed directly toward the center of the Ni_2E_2 diamond core, as does the Cp′Ni a_g combination of d_{z^2} orbitals. Due to this strong spatial overlap, these orbitals interact to form a bonding combination ($1a_g$) and an antibonding combination ($3a_g$*). The $2a_g$ orbital is the Cp′Ni $d_{x^2-y^2}$ orbital combination, which has formal delta symmetry with respect to the Ni−Ni axis, but is essentially nonbonding in view of its long Ni···Ni separations of >3.2 Å in these compounds.

The E−E π bonding orbitals of b_{3u} and b_{1u} symmetry are able to interact with the Cp′Ni $d_{x^2-y^2}$ and d_{z^2} b_{1u} combinations and the d_{xz} b_{3u} combination. Both Cp′Ni b_{1u} combinations are significantly lower in energy and therefore are better energetically matched with the E_2 b_{1u} orbital than the Cp′Ni and E_2 b_{3u} combinations. As a consequence, the orbital interactions of b_{1u} symmetry are much more covalent. In contrast, the Ni_2E_2 b_{3u} orbitals are much more polarized such that the $1b_{3u}$ bonding combination is heavily dominated by E_2 character, and the $2b_{3u}$* antibonding combination may be considered to be a Ni-based orbital. Similar interactions occur in the case of the E−E π^* orbitals of b_{1g} and b_{3g} symmetry, which interact with the b_{1g} Ni d_{xy} and b_{3g} d_{yz} combinations, respectively. Again, the Ni b_{1g} combination lies lower in energy than the b_{3g} combination, yielding greater covalency in the Ni_2E_2 $1b_{1g}/2b_{1g}$* set and greater polarization of the Ni_2E_2 $1b_{3g}/2b_{3g}$* set such that the $2b_{3g}$* orbital may likewise be assigned as primarily a Ni-based orbital.

The final E_2 orbital to be considered is the b_{2u} E−E σ* orbital, which is critical for assessing the oxidation level of the E_2 unit. This antibonding orbital, which matches the Cp′Ni b_{2u} combination of d_{yz} orbitals in both symmetry and energy, gives rise to Ni_2E_2 $1b_{2u}$ and $2b_{2u}$* bonding and antibonding orbitals that are very covalent with similar E_2 and Ni_2 character. A number of Cp′Ni orbitals do not have the appropriate symmetry or energy to interact with the E_2 unit and thereby remain nonbonding. These are the a_u and a_g d_{xy} and $d_{x^2-y^2}$ orbitals, respectively, as well as the b_{2g} combination of d_{xz} orbitals. The $[Ni_2E_2]^{2+}$ unit contributes 26 electrons that are distributed over the molecular orbital manifold shown in Figure 9. The HOMO is the $2b_{1g}$* orbital, which is filled along with the 12 orbitals below it in energy. Three orbitals remain empty: the $2b_{3u}$* LUMO, as well as the $2b_{3g}$* and $2b_{2u}$* orbitals. As we have just discussed, the $2b_{3u}$* and $2b_{3g}$* orbitals may be considered mainly to be Ni-based orbitals, and the $2b_{2u}$* orbital is anticipated to have roughly 50% E_2 and 50% Ni_2 character. On the basis of this approximate analysis, we may assign five holes to the Ni 3d levels and one hole to the E_2 np levels, resulting in oxidation state assignments of $[Ni_2]^{5+}$ and $[E_2]^{3-}$ (i.e., case **B**). Case **A** (Ni^{2+}, E_2^{2-}) would imply the assignment of the $2b_{2u}$* orbital as a Ni orbital, while case **C** implies that this orbital is E_2-centered, with corresponding changes in the assignment of the $1b_{2u}$ orbital. In the sections below, we will test this molecular orbital picture by examination of the results of DFT and multireference CASSCF/CASPT2 calculations. Importantly, agreement between experimental and computational results will be used to validate the calculated electronic structure.

Density Functional Theory Calculations. Geometries for all three $Cp'_2Ni_2E_2$ complexes were optimized using the 100 K crystal structures as a starting point. Structures for analogous Cp″ and Cp compounds, in which Cp″ denotes tetramethylcyclopentadienyl, have also been used in this work, where the simplified structures greatly enhanced the speed of the

Table 6. Bond Distances and Angles from DFT Geometry Optimizations

	E···E (Å)	Ni···Ni (Å)	Ni−E (Å) (avg)	Ni−Cp′ (Å) (avg)	E-Ni-E (deg) (avg)	Ni−E−Ni (deg) (avg)	Cp′−Ni−E_2 (deg) (avg)	Ni−E−E−Ni (deg)
1 $(Cp'NiS)_2$	2.873	3.232	2.162	1.740	83.3	96.7	179.2	180.0
$\mathbf{1}_{red}$ $[(Cp'NiS)_2]^-$	2.817	3.336	2.183	1.776	80.4	99.6	177.5	180.0
2 $(Cp'NiSe)_2$	3.012	3.424	2.280	1.739	82.7	97.3	179.2	179.9
$\mathbf{2}_{red}$ $[(Cp'NiSe)_2]^-$	3.009	3.419	2.290	1.740	82.4	96.8	172.5	166.9
3 $(Cp'NiTe)_2$	3.140	3.602	2.389	1.680	82.2	97.8	177.3	179.8

DOI: 10.1021/ja511607j
J. Am. Chem. Soc. 2015, 137, 4993−5011

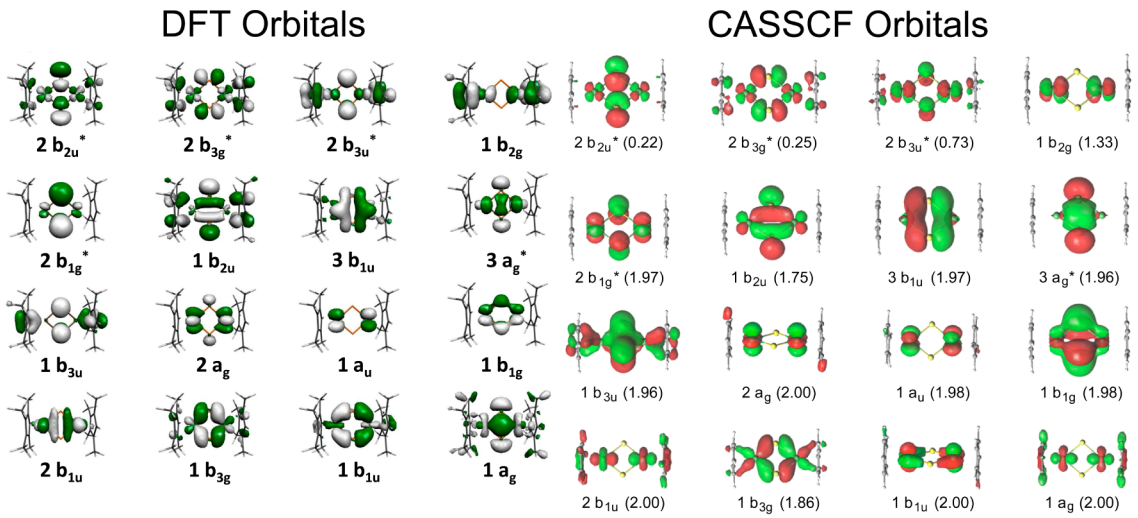

Figure 10. Representative DFT (left) and CASSCF (right) Ni/E orbitals for the $Cp'_2Ni_2E_2$ complexes. The DFT orbitals derive from B3LYP calculations on $Cp''_2Ni_2S_2$, and the CASSCF orbitals come from a calculation on the $Cp_2Ni_2S_2$ complex. Occupation numbers are given in parentheses.

Table 7. Orbital Compositions (%) for $Cp''_2Ni_2E_2$ from Löwdin Analysis of B3LYP Calculations

	E = S			E = Se			E = Te		
	Ni	S	Cp″	Ni	Se	Cp″	Ni	Te	Cp″
$2b_{2u}$*	40.6	40.8	18.6	36.2	47.0	16.8	34.2	51.2	14.6
$2b_{3g}$*	40.3	25.8	33.9	38.6	29.0	32.4	36.6	30.6	32.8
$2b_{3u}$*	42.4	26.6	31.0	40.0	29.4	30.6	40.8	25.8	33.4
$1b_{2u}$	10.2	41.0	48.8	15.0	39.6	45.4	23	36.2	40.8

calculations, the results of which show little differences from those for the Cp′ compounds. The optimized metric parameters for the Cp″ analogues of **1**–**3** are shown in Table 6. In general, good agreement between each calculated and observed geometry is observed, with the largest discrepancy involving the E–E distance. Computationally, these distances are slightly overestimated by only 0.1 Å in the worst case, which could lead to an underestimation of the E–E bonding interaction. The electronic structures of these compounds were calculated using BP86, B3LYP, and PBE functionals, all of which gave similar results regarding orbital ordering and occupation. Slight differences in the energies and compositions of the orbitals were observed but are not detailed here. The calculated (B3LYP) orbital splittings for $Cp'_2Ni_2S_2$, $Cp'_2Ni_2Se_2$, and $Cp'_2Ni_2Te_2$ displayed in Figure S7, Supporting Information, show marked similarity to the anticipated molecular orbital model developed above. The depictions of the B3LYP orbitals (and CASSCF orbitals, vide infra) for $Cp''_2Ni_2S_2$, given in Figure 10, clearly resemble the orbital picture developed above (the corresponding data for $Cp'_2Ni_2S_2$, $Cp''_2Ni_2Se_2$, and $Cp''_2Ni_2Te_2$ are given in Figures S8–S10, Supporting Information). Notably, calculated bond orders for the E···E interactions, using either BP86 or B3LYP under the Mayer or Löwdin formalisms, range from 0.20 to 0.52, consistent with a partial E···E bond.

Representative compositions (B3LYP for the Cp″ complexes) for the $1b_{2u}$, $2b_{3u}$*, $2b_{3g}$*, and $2b_{2u}$* orbitals are given in Table 7 and may be compared with our qualitative expectation that the $2b_{3u}$* and $2b_{3g}$* orbitals are mainly CpNi-based whereas the $1b_{2u}$ and $2b_{2u}$* are best described as highly mixed with roughly equivalent NiCp and E character. Indeed, the E character for the $2b_{3u}$* and $2b_{3g}$* orbitals ranges from 26% to 31%, supporting our qualitative description of these orbitals as mainly CpNi-based. In contrast, the $1b_{2u}$ and $2b_{2u}$* orbitals are highly covalent, having ∼36–51% E_2 character. Interestingly, the percent E_2 character in the $1b_{2u}$ decreases as the size of E increases. This trend suggests that the Ni_2S_2 compound is the most covalent (most S_2^{3-}-like) of the series and that the Ni centers become slightly more oxidized as the size of E increases. Importantly, these minor variations in orbital composition do not manifest themselves in the Ni XAS spectra such that compounds **1**–**3** may all be described chemically as having the same Ni oxidation states.

The validity of the calculated electronic structures is tested not only by their ability to reproduce the observed bond distances in the compounds but also by comparing calculated and experimental spectral features. Experimental and calculated near-IR absorption spectra of the $Cp'_2Ni_2E_2$ species highlighting their two lowest-energy absorptions are shown in Figure 11. Compounds **1** and **2** show a somewhat unsymmetrical low-energy, low-intensity band below 8000 cm^{-1}, referred to here as band I. The peak maxima for **1** and **2** are 7520 and 6850 cm^{-1}, respectively. Additionally, a higher-intensity band at ∼14 000 cm^{-1} is observed (band II). Both features are reproduced by TD-DFT methods in good quantitative agreement with the experimental data, as shown in Figure 11 and Table 3.

For each compound, band I may be ascribed to a $^1A_{1g} \rightarrow {}^1B_{2u}$ transition that primarily involves the $2b_{1g}$* HOMO and the $2b_{3u}$* LUMO. Formally, these are ligand-to-metal charge transfer (LMCT) transitions, as they are predominately E_2 π^* → Ni–E π^* in character. Band II is a $^1A_{1g} \rightarrow {}^1B_{1u}$ transition. Multiple electron configurations give rise to this $^1B_{1u}$ state; hence, this transition is composed of heavily weighted

DOI: 10.1021/ja511607j
J. Am. Chem. Soc. 2015, 137, 4993–5011

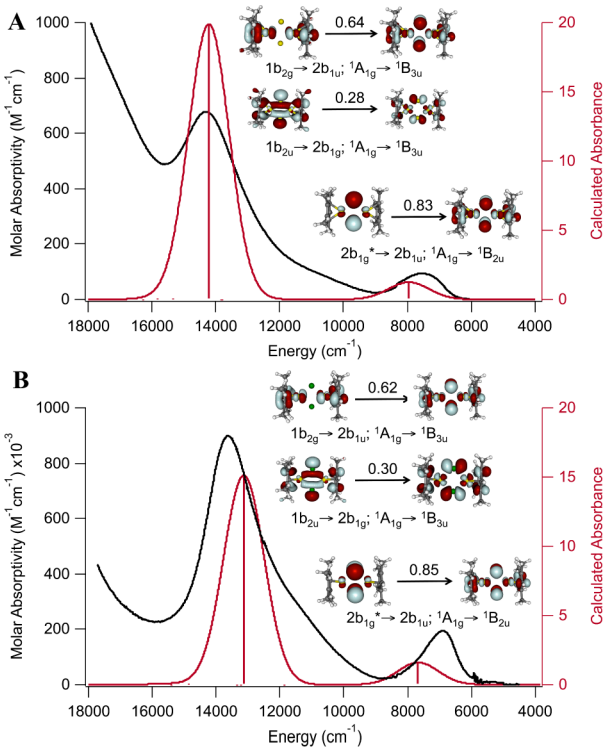

Figure 11. Experimental and TD-DFT calculated near-IR absorption spectra for $Cp'_2Ni_2S_2$ (A) and $Cp'_2Ni_2Se_2$ (B).

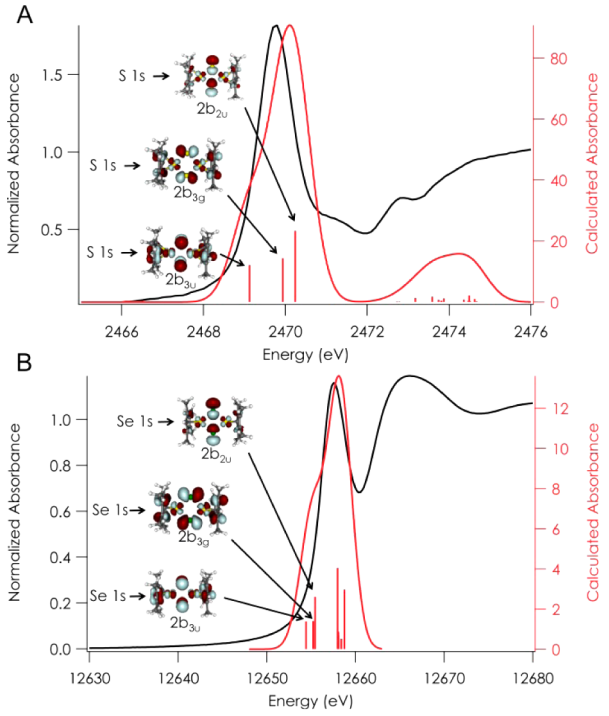

Figure 12. Experimental and TD-DFT calculated S and Se K-edge X-ray absorption spectra of $Cp'_2Ni_2S_2$ (A) and $Cp'_2Ni_2Se_2$ (B).

excitations from multiple MOs. Classification of this transition is not straightforward, though we note that there is significant Ni → Ni as well as Ni → E character.

Both bands I and II are notably unsymmetrical in their appearance. Band I appears "cut off" at energies beyond λ_{max} in a manner somewhat reminiscent of intervalence charge transfer (IVCT) transitions beyond the class II limit. Additionally, band II features a shoulder to lower energy, ~12 000 cm^{-1}, which increases in intensity as E is changed from S to Se. This increase in intensity with atomic number suggests that the shoulder features may be due to singlet-to-triplet transitions, whose intensities are strongly affected by spin−orbit coupling. Indeed, a TD-DFT calculation of triplet excitations for the Se congener predicts bands at 8000, 9400, 10400, 10500, 11500, 12600, and 13500 cm^{-1}. Thus, we may attribute the band asymmetries in these low-energy excitations to the appearance of spin-forbidden transitions, although vibronic coupling may also play a role.

Although the calculated excitation energies have superb agreement with experimental energies, the relative calculated absorptivities do not follow the experimental trend of increased intensities for Se > S. This issue may partially be explained by the triplet excitations, just discussed, but is also likely due to the computational underestimation of the E−E bonding described above.

The S and Se K-edge spectra of $Cp'_2Ni_2E_2$ were both calculated using DFT (BP86/TZVP-ZORA) methods. The results are presented in Figure 12. In both cases, the calculated spectrum predicts a low-energy shoulder that is not observed in the experimental spectrum. This shoulder arises from the S (Se) 1s → ψ(Ni + Cp′ + S (Se)) unoccupied orbitals. These shoulders are likely unobserved experimentally due to core−hole relaxation phenomena that lead to significant line broadening that is not taken into account by the DFT methods. Functional dependence of the S XAS spectrum was explored in calculations using a B3LYP/TZVP-ZORA single-point solution, which yields poorer agreement with experiment. Nonhybrid functionals have been demonstrated to give better agreement with experiment in the calculation of S K-edge XAS data, with a deviation from experiment (after linear energy correction) of 0.12 eV relative to that of 0.44 eV for B3LYP.[28c] The summed oscillator strengths of the BP86-calculated S K-edge excitations are 0.00464. According to the DeBeer/Neese calibration,[28c] this should correspond to an experimental peak area of 4.03 units; the experimental peak area is 4.23. The general agreement between experimental and calculated spectral features here lends significant credence to the electronic structure determined here using DFT.

We have also used DFT to predict vibrational frequencies of the $Cp'_2Ni_2S_2$ compound that are sensitive to the $^{32/34}$S isotopic substitution. There are four such vibrations that are Raman active; these are given in Table 8. Only one of these modes is observed experimentally. The observed vibration appears at 405.8 cm^{-1}. From its energy and the isotopic shift, this vibration matches up best with the predicted B_g (4) mode at 389 cm^{-1}, which has S−S rocking character, although a more in-depth study will be needed for a definitive assignment. The general motion of this vibrational mode is shown in Chart 1. We note that neither the observed mode nor any of the other calculated modes is a pure S−S stretch, so that a direct comparison with S−S stretching modes in S_2^{2-}, S_2^{-}, and S_2^{0} species is not truly appropriate. However, we do note that all of the calculated isotopically sensitive modes appear significantly lower in energy than those of the S−S stretch in genuine S_2^{2-} species (typically at ~446 cm^{-1}), indicating a significantly weaker S−S bonding interaction, as in case **B**.

One final validation of the DFT methods presented here is the calculation of the geometry and EPR g values of the reduced $[Cp_2Ni_2E_2]^-$ monoanions. Characteristic bond dis-

DOI: 10.1021/ja511607j
J. Am. Chem. Soc. 2015, 137, 4993−5011

Table 8. Calculated and Experimental Raman Active Vibrations of $Cp'_2Ni_2S_2$ (symmetry assignments are based on idealized C_{2h} symmetry)

symmetry	^{32}S, cm^{-1}	^{34}S, cm^{-1}	Δ, cm^{-1}	assignment
Calculated Raman Active Modes				
A_g (1)	117	116	1	S−S stretching, Ni−Ni stretching, Cp′ breathing
A_g (3)	292	287	5	S−S stretching, Ni−Cp′ stretching
B_g (4)	389	383	6	S−S rocking
A_g (5)	427	423	4	S−S stretching, Ni−Cp′ stretching
Experimental Raman Data				
B_g (4)	405.8	398.1	7.7	

Literature S−S Stretching Data

species	ν(S−S), cm^{-1}	reference
S_2	718	37
S_2^-	601	38
S_2^{2-}	446	39

Chart 1

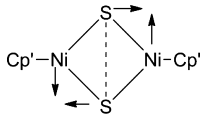

B_g (4)

tances for the optimized geometries of these species having E = S and Se are given in Table 6. The reduced complex anions $[Cp_2Ni_2E_2]^-$ are very similar in geometries to those of the neutral complexes. The largest discrepancy between the DFT calculations and the experimental crystal structures is found for the predicted change in the Se−Se bond length upon reduction as well as the calculated planarity of the Ni_2E_2 cores. Due to the inaccuracy of the calculated Se−Se distance in **1** discussed above, the corresponding distance in **2red** actually matches better the experimental result. The calculated planarity of the Ni_2E_2 cores supports our assumption that their experimental nonplanarity results from crystal packing effects.

The SOMO of **1red** and **2red** has Ni−E antibonding character as well as E···E π bonding character. Thus, the addition of an electron to this orbital is expected to increase the Ni−E distances and shorten the E···E distances. In the DFT geometry-optimized structures of **1**/**1red** and **2**/**2red**, this is what occurs. However, the crystal structure geometries of **1red** and **2red** have E···E distances that are slightly longer than in the neutral compounds. While this discrepancy can mainly be attributed to the computational underestimation of the E···E bonding interactions in **1** and **2** discussed above, it does not provide an explanation for why the E···E distances actually elongate experimentally. In this case, the E···E distance is affected more by the change in the Ni−E distances (a strong antibonding interaction in the SOMO of **1red**/**2red**) than by any residual E···E π bonding interaction, which must be weak at such long E···E separations. Since the DFT calculations underestimate the E···E bonding in **1** and **2**, and more correctly estimate E···E bonding in **1red** and **2red**, the result, counter to experiment, is a shortening of the E···E distances upon reduction.

In Table 9 we collect the charges and spin populations computed for the Cp ring and the Ni and E = S, Se atoms with the PBE functional. The charge distributions obtained from the B3LYP hybrid functional are very similar and do not show any qualitative differences. Effective atomic charges are displayed for three different density partitioning methods, namely, the Mulliken analysis,[40] the Voronoi deformation density (VDD) method,[41] and the Bader Atoms-in-Molecules theory.[42] The absolute charge values vary substantially between the different partitioning methods; in particular the Mulliken approach should be handled with care. However, all methods show the same trend with an analogous behavior for the reduction of the complexes. It is convenient to consider the charge on the combined CpNi unit because of the strongly covalent CpNi bonding interactions. While the charge on both the CpNi unit as well as the E atoms decreases upon formation of the anion from the neutral compound, the change is more drastic for the CpNi unit than it is for the E atoms by roughly a factor of 2, and reduction may be assigned as being essentially localized on the CpNi units, in agreement with case B. Further parsing this charge into Ni and Cp components indicates that it is the Cp ligands that absorb most of the negative charge.

Table 9. PBE/TZP Charges (Q) and Spin Populations ($\alpha-\beta$) per Half-Dimer As Calculated with Three Partitioning Schemes

	Ni		Cp		CpNi		E	
	Q	$(\alpha-\beta)$	Q	$(\alpha-\beta)$	Q	$(\alpha-\beta)$	Q	$(\alpha-\beta)$
Mulliken								
$Cp_2Ni_2S_2$	−0.05	–	0.15	–	0.10	–	−0.10	–
$[Cp_2Ni_2S_2]^-$	0.04	0.30	−0.26	0.09	−0.22	0.40	−0.28	0.10
$Cp_2Ni_2Se_2$	0.03	–	0.13	–	0.15	–	−0.15	–
$[Cp_2Ni_2Se_2]^-$	0.11	0.31	−0.26	0.09	−0.15	0.41	−0.35	0.09
VDD								
$Cp_2Ni_2S_2$	0.23	–	0.01	–	0.24	–	−0.24	–
$[Cp_2Ni_2S_2]^-$	0.20	–	−0.33	–	−0.13	–	−0.37	–
$Cp_2Ni_2Se_2$	0.20	–	−0.01	–	0.19	–	−0.19	–
$[Cp_2Ni_2Se_2]^-$	0.17	–	−0.33	–	−0.16	–	−0.34	–
Bader								
$Cp_2Ni_2S_2$	0.58	–	−0.16	–	0.42	–	−0.42	–
$[Cp_2Ni_2S_2]^-$	0.57	0.33	−0.50	0.09	0.07	0.42	−0.57	0.08
$Cp_2Ni_2Se_2$	0.53	–	−0.18	–	0.35	–	−0.35	–
$[Cp_2Ni_2Se_2]^-$	0.53	0.33	−0.52	0.09	0.02	0.42	−0.52	0.08

DOI: 10.1021/ja511607j
J. Am. Chem. Soc. 2015, 137, 4993−5011

Figure 13 shows isosurface plots of the $2b_{3u}$* LUMO in $Cp_2Ni_2S_2$ and the spin density in the reduced complex anion,

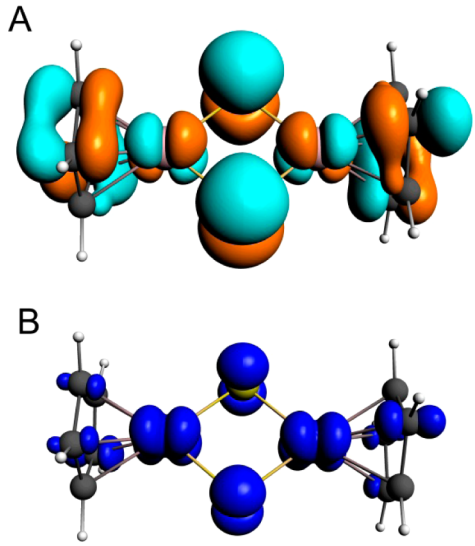

Figure 13. Isosurface plots of (A) Calculated LUMO ($2b_{3u}$*) of $Cp_2Ni_2S_2$. (B) Calculated spin density of $[Cp_2Ni_2S_2]^-$.

$[Cp_2Ni_2S_2]^-$. The LUMO and spin density for the Se complex (not shown) are very similar. The spin density resembles the shape of the LUMO but relaxes such that the majority of the spin density is located on the Ni and E atoms. This is in contrast to the charge, which mainly ends up on the Cp ligands. The Cp ligands thereby act as a charge buffer: the unpaired electron ends up on the Ni_2X_2 group, and at the same time the paired electron density redistributes such that the charge on the metal centers remains close to what it is in the neutral complex. This phenomenon is not uncommon behavior for redox processes of transition metal complexes and is somewhat reminiscent of the concept of "electroneutrality balance" recently discussed by Wolczanski and co-workers.[43]

The calculated EPR g values for the $[Cp_2Ni_2E_2]^-$ complex anions, Table 10, are in good agreement with experiment,

Table 10. EPR g Tensor Values (principal axis representation) for $[Cp'_2Ni_2E_2]^-$ Anions

	g_1	g_2	g_3
$[Cp'_2Ni_2S_2]^-$			
PBE/TZP	2.028	2.066	2.152
PBE/TZP (ZORA)	2.024	2.061	2.150
experiment	2.059	2.067	2.112
$[Cp'_2Ni_2Se_2]^-$			
PBE/TZP	2.025	2.152	2.206
PBE/TZP (ZORA)	2.030	2.148	2.194
experiment[a]	2.05	2.16	2.23

[a]Data from ref 15.

which underpins the reliability of the DFT results. Inclusion of relativistic effects using the ZORA method yields results that are not significantly different from the nonrelativistic results.

We note here that the $[Cp'_2Ni_2S_2]^-$ anion is essentially isovalent with the heterobimetallic $[NiS_2Pt]$ complex with an $S = 1/2$ ground state recently reported by Kaupp, Driess, and co-workers.[21] In the $[NiS_2Pt]$ complex, the calculated S spin density of ~0.4 was taken to indicate that the compound has overall ~40% S_2^{3-} "radical" character. This analysis is inappropriate, since it makes the assumption that any spin density on the S_2 unit arises from the S∴S σ* orbital. In fact, the S spin density in both the $[Cp'_2Ni_2S_2]^-$ anion and the $[NiS_2Pt]$ complex resides mainly in an orbital of S−S π* rather than σ* symmetry, the $2b_{3u}$* orbital in **1**. It is thus not appropriate to assign this spin density as being indicative of S_2^{3-} character. It is instead due to the occupation of an orbital that is mainly Ni-based with significant Ni−S antibonding character. The S∴S σ* "radical" in both compounds forms a strong bond with the metal atoms and is therefore not the highest energy occupied orbital. The idea that a "genuine" S_2^{3-} compound must have purely S-centered spin density is not correct when it is possible for the S−S σ* orbital to interact strongly with metal-centered orbitals, as in **1**, which is diamagnetic and therefore has zero spin density at all points in space.

Multireference Calculations. In cases where the energetic splittings between filled and empty orbitals are small, the ground state of a compound may have contributions from several limiting electronic configurations, a so-called multireference state. Generally, DFT methods poorly describe multireference states, and wave function methods must be employed that use multiple determinants to describe all possible configurations that contribute to the ground state. The DFT calculations presented above showed indications of low-lying excited states, which commonly indicate multireference states. Nevertheless, DFT is able to reliably reproduce many of the salient spectroscopic features of the $Cp_2Ni_2E_2$ compounds. For the sake of completeness and thoroughness, though, we have opted to investigate these compounds additionally using multireference[44] methods, which have yielded further insights into the bonding in these compounds.

In the CASSCF approach used here, the multireference wave function is pieced together from the occupancy numbers of a set of active space orbitals, which are allowed to take on noninteger values between zero and two. The ideal active space for $Cp_2Ni_2S_2$ would be composed of all the valence orbitals of the $(Ni_2S_2)^{2+}$ diamond core including linear combinations of the Ni 3d and 4s orbitals as well as the 3p orbitals on the S atoms. This means that the active space would contain a total of 26 electrons, namely, 9 valence electrons from each Ni^+ atom and 4 valence electrons from each set of S 3p orbitals. In total we would have a CAS of (26e/18o). Unfortunately, an active space of this size is computationally unfeasible due to the large amount of configuration state functions involved. It is clear from the molecular orbital analysis above that the 4s orbitals will be empty and can be safely removed from the active space. From a simple Hartree−Fock calculation, we noticed that the $3d_{z^2}$−$3d_{z^2}$ bonding ($1a_g$)/antibonding ($2b_{1u}$) pair is fully occupied with electrons and lies low in energy, such that these two orbitals and four electrons can be removed. A similar procedure can be performed with one of the two filled bonding ($2a_g$)/antibonding ($1b_{1u}$) pairs of δ symmetry derived from the $3d_{x^2-y^2}$ orbitals. The other ($3d_{xy}$) δ-type pair (b_{1g}/a_u orbitals) has some significant mixing with the s orbitals, and we have included it in the active space. On the basis of these considerations, we reach a space of (18e/12o). We have calculated five excited states for each irreducible representation: a total of 20 transition energies for the singlet and 20 transition energies for the triplet excited states.

The CASSCF orbitals and their occupation numbers for the ground state are given in Figure 10. These orbitals are

DOI: 10.1021/ja511607j
J. Am. Chem. Soc. 2015, 137, 4993−5011

Table 11. Predicted (from DFT/PBE/def2-TZVPP) Features of the Entire Series of $Cp_2M_2S_2$ Compounds for All First-Row Transition Metals

$Cp_2M_2S_2$		spin state	M···M, Å	S···S, Å	M−S, Å	charge	spin	natural electron configuration
$Cp_2Zn_2S_2$	Zn	$S = 0$	4.003	2.375	2.327	1.57	0.00	$(4s)^{0.37}(3d)^{9.97}$
	S					−0.77	0.00	$(3s)^{1.90}(3p)^{4.81}$
$Cp_2Cu_2S_2$	Cu	$S = 0$	3.804	2.252	2.211	0.99	0.00	$(4s)^{0.32}(3d)^{9.64}$
	S					−0.45	0.00	$(3s)^{1.87}(3p)^{4.52}$
$Cp_2Ni_2S_2$	Ni	$S = 0$	3.301	2.708	2.134	0.65	0.00	$(4s)^{0.36}(3d)^{8.94}$
	S					−0.37	0.00	$(3s)^{1.86}(3p)^{4.47}$
$Cp_2Co_2S_2$	Co	$S = 1$	3.182	2.856	2.138	0.43	0.80	$(4s)^{0.37}(3d)^{8.15}$
	S					−0.28	0.10	$(3s)^{1.84}(3p)^{4.40}$
$Cp_2Fe_2S_2$	Fe	$S = 1$	2.585	3.326	2.106	0.15	0.95	$(4s)^{0.33}(3d)^{7.45}$
	S					−0.07	0.02	$(3s)^{1.82}(3p)^{4.21}$
$Cp_2Mn_2S_2$	Mn	$S = 0$	2.545	3.354	2.105	−0.10	0.00	$(4s)^{0.34}(3d)^{6.69}$
	S					0.08	0.00	$(3s)^{1.78}(3p)^{4.10}$
$Cp_2Cr_2S_2$	Cr	$S = 1$	2.600	3.438	2.155	0.01	1.00	$(4s)^{0.31}(3d)^{5.61}$
	S					−0.01	0.00	$(3s)^{1.78}(3p)^{4.19}$

qualitatively similar to those obtained through DFT calculations. Examining the orbital occupation numbers, we see from the six highest-energy orbitals that the $(1b_{2u})^2(1b_{2g})^2(2b_{1g}^*)^2(2b_{3u}^*)^0(2b_{3g}^*)^0(2b_{2u}^*)^0$ configuration, which is the same configuration obtained from DFT, clearly makes the largest contribution to the wave function. Surprisingly, however, for **1** the contribution is only 33%, and many other configurations make up the remaining 67% of the wave function.[45] Compounds **2** and **3** are similarly mixed, with the main electron configuration making up 35% and 31% of the wave function, respectively. The source of this multireference character appears to be static correlation between energetically proximate electronic states of the molecule. Considering the degree of multireference character of these compounds, it is remarkable that DFT is able to provide such an accurate prediction of their properties.

Having described the multireference wave function, we may now turn to the question of E−E bonding in the Ni_2E_2 compounds. Clearly, for **1** and **2**, the main $(1b_{2u})^2(1b_{2g})^2(2b_{1g}^*)^2(2b_{3u}^*)^0(2b_{3g}^*)^0(2b_{2u}^*)^0$ configuration of the wave function, as discussed above, is most consistent with the formulation of a $[Ni_2]^{5+}/[E_2]^{3-}$ species with an E−E half σ bond. In order to give full consideration to the many other electron configurations that make up the ground-state wave function, we may use the occupation numbers for each orbital, since they are summed up for all configurations that contribute to the wave function. In this manner, the six highest orbital occupancies are the following: $(1b_{2u})^{1.75}(1b_{2g})^{1.33}(2b_{1g}^*)^{1.97}(2b_{3u}^*)^{0.73}(2b_{3g}^*)^{0.25}(2b_{2u}^*)^{0.22}$. Obviously, there are significant deviations from the leading configuration that have a strong influence on the nature of the Ni−S σ and π bonding in **1**. However, if we concern ourselves solely with the question of S−S bonding, we may note that the occupancies of the $1b_{2u}$ and $2b_{2u}^*$ orbitals are fairly similar to those in the leading configuration. Moreover, the sum of the occupancies of these orbitals is 1.75 + 0.22 = 1.97, indicating that only two electrons occupy this set of orbitals. As before, we may assign these electrons as deriving from the union of the S_2^{3-} ligand with the $(Ni_2)^{5+}$ metal centers.

Quantized Oxidation States, or a Continuum of E···E Bonding Interactions? The structures **A**, **B**, and **C** shown in Scheme 3 are limiting resonance structures for the electronic structures of **1**−**3**. It is tempting to imagine that these structures represent signposts along a continuum of structures having varying amounts of S−S interaction, and that the true electronic structure for any given compound most likely lies somewhere between these limiting structures along such a continuum. This notion is especially appealing in the case of organometallic compounds, where variable amounts of π back-bonding are well-known to give rise to such a bonding continuum in π-acceptor ligands such as CO or N_2.[46] However, we must keep in mind that the E_2^{n-} ligands are π-donor ligands and not π-acceptors. Thus, the issue of π back-bonding is not germane to the nature of their bonding to transition metals, even in organometallic compounds.

To investigate the nature of E−E bonding more generally among compounds having an M_2S_2 diamond core, we have performed DFT calculations on an entire series of hypothetical $Cp_2M_2S_2$ compounds where the M element was varied across the first-row of transition metals from Cr to Zn. Calculated structural details for these compounds in their lowest-energy spin states are given in Table 11. Changes in calculated atomic charges and natural electron configuration values across the series are smooth and expected. However, the bond distances across this series show an unusual trend (Figure 14). A plot of the M···M separations against the S···S distances, rather than being a continuous curve, shows clustering of the compounds into three distinct categories. As indicated in Figure 14, we suggest that these are $[M_2]^{4+}/[S_2]^{2-}$, $[M_2]^{5+}/[S_2]^{3-}$, and $[M_2]^{6+}/[S_2]^{4-}$ species. With the exception of the Ni complex, none of the other $Cp_2M_2S_2$ compounds has experimental precedent. Thus, this list suggests some rather intriguing synthetic targets. We have attempted the synthesis of the Se analogue of the Co complex, predicted to be a Se_2^{3-} complex, but instead have obtained a $[Cp_3Co_3(Se_2)_2]$ compound somewhat analogous to the previously reported $[Cp_3Ni_3(Se_2)_2]^+$ species.[15,47]

We have also expanded upon this analysis to catalogue all known first-row transition metal compounds with a planar M_2S_2 core that are reported in the Cambridge Structural Database (CSD); a plot of their M···M separations vs S···S distances is also shown in Figure 14. A similar analysis of M_2Se_2 compounds may be found in Supporting Information (Figure S12); there are too few known M_2Te_2 compounds to complete such an analysis in the case of Te. In contrast to a similar cataloguing of metal−N_2 complexes from the CSD, which shows a smooth, continuous curve,[46] clustering is again observed for the M_2S_2 compounds. The large majority of

DOI: 10.1021/ja511607j
J. Am. Chem. Soc. 2015, 137, 4993−5011

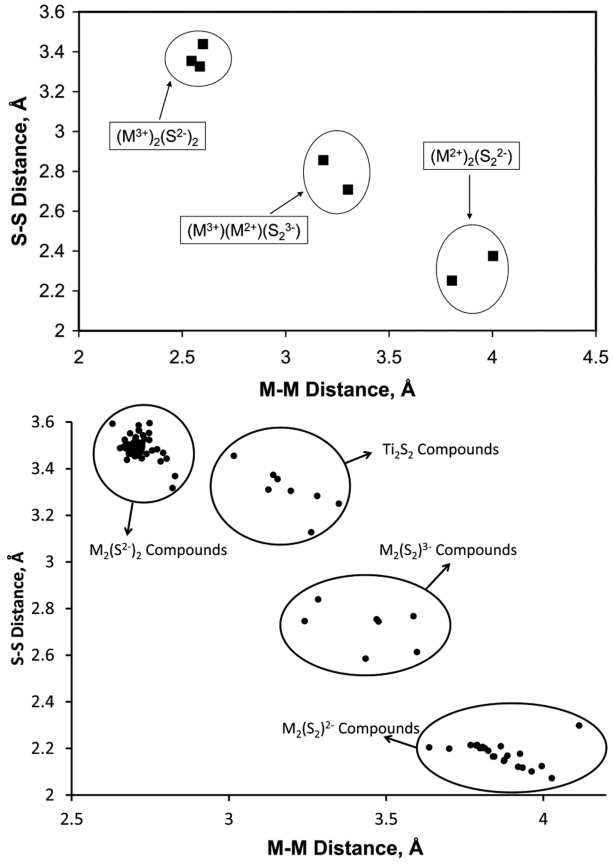

Figure 14. Structural data of the M_2S_2 diamond core for all calculated $Cp_2M_2S_2$ compounds with M = Cr−Zn organized as a function of the M···M and S···S distances in the compounds (top), and corresponding data for all compounds registered in the Cambridge Structural Database (bottom).

compounds can clearly be identified as either disulfido (S_2^{2-}) or sulfido ($2 \times S^{2-}$) compounds. There are two other clusters of compounds in the CSD data, however. There is a class of metal sulfido compounds with extraordinarily long M···M separations between 3 and 3.5 Å. These are all complexes of Ti(IV),[48] and the extra-long M···M distance is likely an effect of the electrostatic repulsion between two highly charged M^{4+} ions that would not appear elsewhere in the first row of the transition metals.

The last class of known compounds has intermediate M···M and S···S separations, and compound **1** belongs to this cluster. As **1** can be assigned as a compound containing the S_2^{3-} subsulfido ligand, we likewise suggest that the other compounds in this class, shown in Chart 2, are also subsulfido compounds.[49] Noteworthy is that the $[Cu_3S_2]$ and $[NiS_2Pt]$ compounds discussed earlier have been described in the literature as having S oxidation states between the S_2^{3-} and sulfide states.[19,21] Deviations from integer (or half-integer) oxidation levels undoubtedly occur at the limit of covalent bonding; however, the extensive crystallographic data presented in Figure 14 suggest that, to a first approximation (arguably, the level most useful for chemists), these compounds are best classified as subsulfide compounds.

With the data in Figure 14 and Figure S13, Supporting Information (the corresponding plot for second and third row transition metals), we may at this point be prescriptive about the structural features that may be said to define a S_2^{3-} complex

Chart 2. Known Compounds That May be Reassigned As Containing S_2^{3-} Ligands

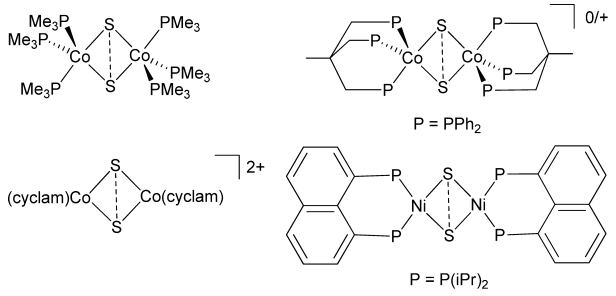

(see Chart 3). For first row transition metals (excluding Ti^{4+}), the shortest nonbonded S···S distance between sulfide ligands is

Chart 3. Ranges of S···S Distances for the Three Classes of M_2S_2 Compounds[a]

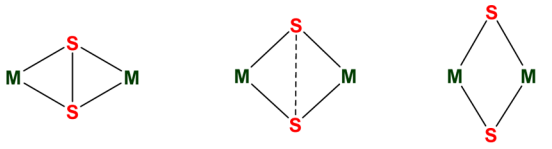

Disulfides	Subsulfides	Sulfides
2.0 Å < d(S-S) < 2.3 Å	2.5 Å < d(S-S) < 2.9 Å	d(S-S) > 3.0 Å

[a]As mentioned in the text, these distances apply to compounds of the first-row transition metals.

~3.3 Å, and the longest S−S bond distance for disulfides is ~2.3 Å. Voids in the crystallographic data for S···S distances of 3.3−2.8 Å and 2.5−2.3 Å indicate that the compounds with S···S distances of 2.5−2.8 Å belong to a separate class, which we can refer to as S_2^{3-} compounds. For second and third row metals (Figure S13, Supporting Information), the atomic radii of the metals are larger, so the ranges of distances are correspondingly larger. Excluding the high oxidation state early metals (Zr^{4+} and Ta^{5+}), the shortest nonbonded sulfide S···S distance is >3.4 Å, and there appear to be no genuine examples of S_2^{2-} compounds. But there is a second class of compounds of late transition metals with S−S distances between 2.9 and 3.1 Å that could be S_2^{3-} compounds, although a separate investigation into the nature of this class of compounds would be needed for a definitive assignment.

What about oxygen? Data from a similar scan of the CSD for first-row transition metal M_2O_2 complexes are shown in Figure S14, Supporting Information. The overwhelming majority of compounds are oxides, and subgroupings into those with metal oxidation states of +2, +3 and those with oxidation states >+3 is possible. Very few peroxo complexes are structurally characterized, and there is a large void in the M−M/O−O plot at intermediate distances where "suboxide" O_2^{3-} species would be expected to appear. At this time, there are no experimental data to suggest the existence of an O_2^{3-} complex, and there are a number of reasons why such a species may not be stable. Electron−electron repulsion in such a highly charged anionic ligand would certainly be greater than in the case of the heavier chalcogens, and 2p orbital overlap will be significantly less than *n*p overlap with $n > 2$. These issues would result in disproportionation of an O_2^{3-} species. We can only wonder

DOI: 10.1021/ja511607j
J. Am. Chem. Soc. 2015, 137, 4993−5011

at this point if supporting ligands could be designed that will overcome these obstacles and stabilize a suboxide complex.

Summary. The electronic structures of **1**−**3** have been investigated using a number of complementary methods aimed at providing "physical" oxidation states to the Ni and chalcogen atoms in the $Cp'_2Ni_2E_2$ structures. We consider three possible assignments for the compounds: case **A**, in which oxidation states of Ni(II) and $(E_2)^{2-}$ may be assigned with an E−E single bond; case **B**, where a mixed-valent Ni_2(II,III) core is combined with the unusual three-electron half-bonded $(E_2)^{3-}$ ion; case **C**, in which no E−E bond exists, and two Ni(III) ions are bridged by two E^{2-} ligands. High quality, low-temperature crystallographic data indicate that each compound has an E···E distance that lies between what is expected for case **A** and case **C**, but would be consistent with case **B**. Information from ^{77}Se and ^{125}Te NMR spectroscopy do not allow for an unambiguous assignment but do disfavor case **A** in the Se compound. Ni K-edge X-ray absorption spectra (XAS) of **1**−**3** are closely similar, indicating very similar electronic structures for the three compounds. Se XAS data for **2** were compared with a number of Se compounds of known oxidation states, providing a strong correlation between the energy of the Se K edge and the Se oxidation state. This calibration curve gives rise to a Se oxidation state of −1.5 for **2**, consistent with case **B**. Compound **1** shows a band in its resonance Raman spectrum at 406 cm^{-1} that is sensitive to $^{32}S/^{34}S$ isotopic substitution. This band is too low in energy to be associated with an $(S_2)^{2-}$ ligand, which disfavors assignment to case **A**.

Chemical reductions of **1** and **2** yield anionic $[Cp'_2Ni_2E_2]^-$ compounds, **1red** and **2red**. These have been shown crystallographically to have E···E distances that are very similar to those in **1** and **2**, respectively, suggesting that the E_2 unit is not reduced. S K-edge XAS data agree with this assessment in that the S K-edge energy is not changed between **1** and **1red**. The pre-edge feature in the S K-edge XAS shifts to higher energy, as is expected for a decrease in the oxidation state of the Ni. The ∼2 eV shift to lower energy of the 1s → 4p + LMCT transition in the Ni K-edge XAS data of **1red** vs **1** is also in accord with a lower Ni oxidation state in **1red** than in **1**. X-ray photoelectron spectra (XPS) in the Ni $2p_{3/2}$ region of the spectrum show a similar shift to lower energy between **1red** and **1**, also indicative of a lower Ni oxidation state in **1red**. EPR spectra of **1red** and **2red** are similarly rhombic and do not show any distinct hyperfine structure.

All of the data discussed herein provide a self-consistent picture of the electronic structures of the compounds investigated. Compounds **1**−**3** are best described as case **B** compounds containing the unusual subchalcogenido ligands, $(E_2)^{3-}$, and a fully delocalized, class III mixed-valent Ni_2(II,III) core. Chemical reduction to **1red** and **2red** is Ni-centered, leaving the $(E_2)^{3-}$ ligands intact, but changing the Ni oxidation states to Ni_2(II,II).

Computational results on **1**−**3** at the DFT and CASSCF levels of theory have provided further insights and details about the bonding in these structures. The Ni−chalcogen bonding is quite covalent, thwarting various approaches to assess the nature of a "localized" E−E bond. Instead, the full manifold of Ni d orbitals and E p orbitals and their interactions must be taken into account. The central issue of the electronic structure of **1**−**3** is the question of what happens with the E−E σ^* orbital. In each of these compounds, the E−E σ^* orbital of b_{2u} symmetry is closely energetically matched to pair with a Ni_2 b_{2u} set forming bonding ($1b_{2u}$) and antibonding ($2b_{2u}^*$) combinations having split Ni and E character. Formally, the $1b_{2u}$ orbital is filled, and the $2b_{2u}^*$ is empty; thus, it is reasonable to assign one of the $1b_{2u}$ electrons as belonging to Ni and the other as being derived from the E_2 unit. This E_2 $\sigma^*(1)$ assignment is consistent with case **B** and a strongly covalent $(Ni_2^{5+})(E_2^{3-})$ core. Neither the $1b_{2u}$ nor the $2b_{2u}^*$ orbitals are frontier orbitals, and therefore **1**−**3** do not show chalcogen "radical" character as characterized by unpaired spin density in the E−E σ^* orbital; nor do their isostructural monoanions. Importantly, the leading electron configuration of **1**−**3** is shown by CASSCF calculations to only make up 31−35% of the ground state. Nevertheless, occupation numbers for **1** of the $1b_{2u}$ (1.75) and $2b_{2u}^*$ (0.22) orbitals that take into account the multitude of other configurations that contribute to the ground state are still consistent with the view of there being two electrons that occupy the $[(1b_{2u})(2b_{2u}^*)]$ set of orbitals: namely, one from the Ni_2^{5+} unit, and the other from the E_2^{3-} unit.

X-ray crystallography is shown here to be the most decisive method for the identification of compounds that contain E_2^{3-} ligands. A prediction of geometries for $Cp_2M_2S_2$ compounds with M spanning the entire series of first-row transition metals shows clustering of the S···S separations into (1) those that clearly contain either S_2^{2-} ligands or two S^{2-} ligands, and (2) those that contain intermediate S···S distances with electronic structures consistent with S_2^{3-} ligation. Surveys of crystallographic data from the Cambridge Structural Database of all compounds with planar M_2E_2 cores shows similar clustering, rather than a smooth continuum of intermediate E···E distances. Thus, the massive amount of structural data collected to date suggests that E_2 ligands bind to transition metals in quantized redox states, E^{2-}, E_2^{3-}, and E_2^{2-}, rather than displaying a continuum of E−E bonding interactions.

EXPERIMENTAL SECTION

Materials and Methods. All operations were carried out under an atmosphere of pure nitrogen using glovebox or Schlenck techniques. Na_2S_2, $Na_2{}^{34}S_2$,[50] Na_2Se_2,[51] 1,2,3,4-tetraisopropylcyclopentadiene,[52] $(Cp'NiS)_2$ (**1**), $(Cp'Ni^{34}S)_2$ (**1iso**), $(Cp'NiSe)_2$ (**2**), and $(Cp'NiTe)_2$[22a] were prepared according to literature procedures. ^{1}H NMR spectra were recorded on a Bruker-AC 300 spectrometer; ^{77}Se and ^{125}Te NMR spectra were recorded on a Varian INOVA-500 spectrometer. UV−vis−NIR spectra were recorded on a Cary 5000 UV−vis−NIR spectrometer. X-Band EPR spectra of solid **1red** diluted in KBr were recorded at 298 K using a Bruker EleXsys EPT spectrometer E-500-A console with an ER 049SX SuperX Bridge and SuperX Cavity. MALDI mass spectra of **3** were obtained using a Bruker REFLEX II matrix-assisted laser desorption/ionization (MALDI) time-of-flight (TOF) mass spectrometer. MALDI mass spectra of all other compounds were obtained using a Bruker ULTRAFLEX III mass spectrometer using matrix-assisted laser desorption/ionization (MALDI) time-of-flight/time-of-flight (TOF/TOF). Elemental analyses were performed by Midwest Microlab, LLC, Indianapolis, IN.

Crystallographic data were collected at the Molecular Structure Laboratory of the Chemistry Department of the University of Wisconsin—Madison. Crystals were selected under oil at room temperature. All the crystals were attached in turn to the tip of a MiTeGen MicroMount. The crystals were mounted in a stream of cold nitrogen at 100 K and centered in the X-ray beam using a video monitoring system. Crystal evaluation and data collection were performed on a Bruker Quazar SMART APEX-II diffractometer with Mo Kα (λ = 0.1073 Å) radiation. The data were collected using a routine to survey reciprocal space and were indexed by the SMART program.[53] The structures were solved from direct methods and refined by iterative least-squares refinements on F^2 followed by

DOI: 10.1021/ja511607j
J. Am. Chem. Soc. 2015, 137, 4993−5011

difference Fourier synthesis. All hydrogen atoms were included in the final structure factor calculation at idealized positions and were allowed to ride on the neighboring atoms with relative isotropic displacement coefficients.

XPS data were obtained using a custom-built XPS system (Physical Electronics Inc., Eden Prairie, MN) equipped with an Al Kα source (1486.6 eV photon energy), a model 10-420 toroidal monochromator, and a model 10-360 hemispherical analyzer with a 16-channel detector array. Measurements were typically performed using an electron take-off angle of 45° and analyzer pass energy of 58.7 eV. Samples were drop-cast on either silicon wafers (for **2**, **2red**, **3**, and **4**) or gold wafers (for **1** and **1red**) and dried in the glovebox. The dried samples were loaded on an XPS sample holder in the glovebox and sealed in a bottle before being quickly loaded into the XPS chamber. To compensate for any sample charging, the main C(1s) peak was shifted to 284 eV, and all other peaks were shifted by the same amount. After linear and Shirley background removal, the peaks were fit with Voigt functions composed of ∼90% Gaussian and ∼10% Lorentzian character with the software Fityk.[35,54] Errors in the measurement of XPS peak intensity were estimated to be ∼10%. The 2p peaks of the elements were fitted with a fixed 2 to 1 ratio of S($2p_{3/2}$) to S($2p_{1/2}$). Stoichiometries of the elements were calculated with the ratio of the elemental peak intensities corrected with their corresponding atomic sensitivity factors (ASFs).[35]

All the XAS samples were analyzed as solids under anaerobic conditions and diluted in boron nitride. XAS Ni K-edges were acquired at the SSRL beamline 7-3, which is equipped with a Si(220) ϕ = 90° double crystal monochromator, a 9 keV cutoff mirror, and a He cryostat (at 20 K). Data were collected using a PIPS detector with a Z-1 filter. S K-edges were analyzed under a He flow cryostat at beamline 4-3; a Lytle detector was used for data collection. Data averaging and energy calibration were performed using SixPack.[55] The first inflection points from the XANES spectral regions were set to 8331.6 eV for Ni foil (Ni samples), while S K-edge data were calibrated to the maximum of the first peak of $Na_2S_2O_3{\cdot}5H_2O$ at 2472.02 eV. The AUTOBK algorithm available in the Athena software package[56] was employed for data reduction and normalization.

All DFT calculations were performed with either the ORCA[57] software package (BP86[58,59] and B3LYP[60] calculations) or the ADF[61] program (PBE[58,62] and g tensor calculations[63]). The crystal structure of $(Cp'NiS)_2$, **1**, was used to construct two truncated models: namely, $(CpNiS)_2$ (**1m**), in which the isopropyl groups were replaced with hydrogen atoms, and $(Cp''NiS)_2$ (**1mod**), in which the isopropyl groups were replaced by methyl groups, electronically similar to the isopropyl groups in **1** but lacking their steric influence. Geometry optimizations with the BP86 functional[58,59] and the PBE[58,62] functional were performed on both **1m** and **1mod** with no symmetry constraints and either a Gaussian type SVP basis set[64] for ORCA or a larger Slater type TZP basis set from the ADF basis set[65] library with its corresponding fit basis set. All optimizations were found to reproduce experimental bond distances and angles with good accuracy, being robust to both changes in functional and basis sets as well as ligand truncations. Bond distances reported here are for the PBE/TZP[58,62,65] optimizations on **1mod**, for which the largest discrepancy from the experimental structure of **1** is the Se−Se distance, which was overestimated by ∼0.05 Å (Table 6). The electronic structure was analyzed at each optimized geometry using both the pure DFT functional as well as the hybrid B3LYP[60] functional. The electronic structures showed minimal changes due to ligand truncations, differences in basis sets, and differences in functional. The electronic structures were also found to be stable with respect to open-/closed-shell solution; broken symmetry methods converged to the same wave function as those for the closed-shell calculations. Orbitals were visualized using the MOLEKEL program.[66] TDDFT calculations of electronic absorption spectra were initiated starting from converged solutions of spin-restricted DFT calculations that employed the B3LYP[60] functional with the TZVP[65] basis along with the Tamm−Dancoff approximation. B3LYP[60] calculations employed the chain-of-spheres approximation (RIJCOSX). Single-point calculations incorporated scalar relativistic effects with the zeroth order regular approximation (ZORA).[67] XAS spectra were calculated according to a previously established time-dependent DFT (TDDFT) protocol that uses the BP86 functional.[28c]

Additional ab initio calculations were performed using the complete active space (CAS) SCF method followed by multiconfigurational second-order perturbation theory (CASPT2). Cp′ rings were substituted with Cp rings in order to facilitate the calculations. Scalar relativistic effects were included using the Douglas−Kroll−Hess Hamiltonian and relativistic ANO-RCC basis set of VTZP quality, as implemented in the MOLCAS 7.7 package.[68] Spin−orbit coupling was included using the complete active space interaction method, CASSI, which employs an effective one-electron spin−orbit (SO) Hamiltonian, based on the mean field approximation of the two electronic part.

In the CASSCF treatment, under C_{2h} symmetry the ideal active space of $Cp_2Ni_2S_2$ would be composed of all the molecular orbitals localized on the Ni_2S_2 ring. This would include the 18 molecular orbitals depicted in Figure 9, 12 of which originate from a linear combination of the five 3d and the 4s AOs localized on each of the nickel atoms and the remaining 6 from the 4p orbitals of the sulfur atoms. This means that the active space would contain a total of 28 electrons [i.e., 10 valence electrons from each Ni atom (ground-state electronic configuration $3d^84s^2$) and 4 valence electrons from the sulfur 2p orbitals of each S atom]. In total we would have a CAS of (28e/18o). Unfortunately, an active space of this size is computationally unfeasible due to the large number of configuration state functions involved. Thus, a consistent truncation of the active space was applied. First, both the empty 4s orbitals for Ni(II) or Ni(III) can be safely removed from the CAS. Simple HF calculations indicated that the $3d_\sigma$-$3d_\sigma$ bonding (a_g)/antibonding(b_u*) orbitals were occupied and low in energy, and so these two orbitals and four electrons were removed from the CAS (but they were still used in the CASPT2 step). The same can be done with one of the two bonding(a_g)/antibonding(b_u*) pairs of δ symmetry: $3d_\delta$-$3d_\delta$. The other δ-type pair has significant mixing with the S orbitals and thereby remains in the active space. On the basis of these considerations, a space of (18e/12o) is achieved. For computational reasons, we have added two empty $4d_\delta$ orbitals to retrieve the double-shell correlation effect. The double-shell effect is considered critical for excited states in order to discern between states that are very close in energy (like the identification of the correct ground state).

Following all these steps, a large but affordable space of (18e/14o) was obtained. Five excited states for each irreducible representation were calculated, i.e., a total of 20 transition energies for the singlet and 20 transition energies for the triplet.

Preparation of Na_2Te_2. Solid Na (0.23 g, 10 mmol) and Te pellets (1.27 g, 10 mmol) were packed inside a carbon-coated quartz tube, which was flame-sealed under vacuum. The tube was placed inside of a high-temperature furnace, which was gradually heated from room temperature to 1100 °C over 4 h. After the sample was heated for an additional 1 h at 1100 °C, the quartz tube was gently placed in ice−water for 15 min. The tube was subsequently transferred into the glovebox, and the contents were collected as bronze colored solids (1.34 g, 89% yield) in agreement with the literature and were used without further characterization.

Characterization of $(Cp'Ni)_2S_2$ (1). ^{1}H NMR (CD_2Cl_2, 300 MHz, ppm) δ 4.74 (s, 2H, ring-CH), 2.93 (sep, 4H, $CHMe_2$), 2.81 (sep, 4H, $CHMe_2$), 1.32 (d, 12H, J_{HH} = 6.6 Hz, CH_3), 1.26 (d, 12H, J_{HH} = 6.3 Hz, CH_3), 1.18 (d, 12H, J_{HH} = 6.9 Hz, CH_3), 1.02 (d, 12H, J_{HH} = 6.3 Hz, CH_3), UV−vis in pentane λ (ε) =320 nm (1790), 394 nm (3310), 464 nm (6900), 730 nm (690), MS (MALDI-MS, 68 eV; m/z (%)), 645.1 ($[\mathbf{1} - H]^+$, 100). Anal. (Calcd C, 64.99%; H, 9.02%. Found C, 65.14%; H, 8. 83%).

Synthesis of $[Cp^*_2Co][(Cp'NiS)_2]$ (1red). A slurry of Cp^*_2Co (214 mg, 0.33 mmol) in 10 mL of MeCN was added to solid $(Cp'NiS)_2$ (87 mg, 0.26 mmol) over 10 min at room temperature, resulting in a black solution, which was stirred overnight. The solvent was then removed under vacuum, and the dark black solid was washed with portions of ∼25 mL of pentane, until the wash became colorless. The resulting solid was extracted with 10 mL of MeCN. The resulting

DOI: 10.1021/ja511607j
J. Am. Chem. Soc. 2015, 137, 4993−5011

mixture was filtered, and the filtrate was collected and evaporated to dryness. The solid was dissolved in a minimal amount of MeCN and stored at −30 °C. Dark red block crystals were collected (65 mg, 25% yield). The compound is unstable in solution. $C_{54}H_{88}Ni_2S_2Co$, (MALDI-MS, 66 eV; m/z (%)), 645.9 ([**1** − H]$^+$, 100), 329.7 ([Cp*$_2$Co]$^+$, 100). $C_{54}H_{88}Ni_2S_2Co$ (15% MeCN). Anal. $C_{54}H_{88}Ni_2S_2Co{\cdot}0.1CH_3CN$ (Calcd C, 66.30%; H, 9.06%. Found C, 66.63%; H, 8.98%).

Characterization of (Cp′Ni)$_2$Se$_2$ (2). ^{1}H NMR (CD_2Cl_2, 300 MHz, ppm) δ 4.67 (s, 2H, ring-CH), 2.92 (sep, 4H, $CHMe_2$), 2.81 (sep, 4H, $CHMe_2$), 1.34 (d, 12H, J_{HH} = 6.6 Hz, CH_3), 1.28 (d, 12H, J_{HH} = 6.3 Hz, CH_3), 1.11 (d, 12H, J_{HH} = 6.9 Hz, CH_3), 0.98 (d, 12H, J_{HH} = 6.3 Hz, CH_3), ^{77}Se NMR (Tol-d_8, 500 MHz), δ 880 (s), UV−vis in pentane λ (ε) = 324 nm (2230), 401 nm (5080), 479 nm (7900), 735 nm (920), MS (MALDI-MS-MS, 68 eV; m/z (%)), 742.19 ([**1** − H]$^+$, 100), 706.08 ([**1** − iPr]$^+$, 14), 524.24 ([**1** − Cp′]$^+$, 18. Anal. (Cp′Ni)$_2$Se$_2$ (Calcd C, 55.03%; H, 7.88%. Found C, 54.97%; H, 7.79%).

Synthesis of (Cp*$_2$Co)$^+$(Cp′Ni)$_2$Se$_2^-$ (2red). A slurry of Cp*$_2$Co (55 mg, 0.17 mmol) in 10 mL of MeCN was added to solid (Cp′Ni)$_2$Se$_2$ (124 mg, 0.17 mmol) over 10 min at room temperature, resulting in a black solution, which was stirred overnight. The solvent was then removed under vacuum, and the dark black solid was washed with portions of ∼25 mL of pentane, until the wash became colorless. The resulting solid was then extracted with 10 mL of MeCN. The mixture was filtered, and the filtrate was collected and evaporated to dryness. The solid was dissolved in a minimal amount of MeCN and stored at −30 °C. Dark green block-shaped crystals were collected (82 mg, 45% yield). The compound is unstable in solution. $C_{54}H_{88}Ni_2Se_2Co$. Anal. (Calcd C, 60.53%; H, 8.28%. Found C, 60.63%; H, 8.08%). EMM (MALDI-MS, 66 eV; m/z (%)), 741.9 ([(Cp*$_2$Co)$^+$(Cp′Ni)$_2$Se$_2^-$ − H]$^+$, 100), 329.7 ([Cp*$_2$Co]$^+$, 40).

Characterization of (Cp′Ni)$_2$Te$_2$ (3). ^{1}H NMR (CD_2Cl_2, 300 MHz, ppm) δ 5.94 (s, 2H, ring-CH), 3.55 (sep, 4H, $CHMe_2$), 3.51 (sep, 4H, $CHMe_2$), 2.03 (d, 12H, J_{HH} = 6.6 Hz, CH_3), 1.86 (d, 12H, J_{HH} = 6.3 Hz, CH_3), 1.81 (d, 12H, J_{HH} = 6.9 Hz, CH_3), 1.69 (d, 12H, J_{HH} = 6.3 Hz, CH_3). ^{125}Te NMR (Tol-d_8, 500 MHz), δ 822 (s), UV−vis in pentane λ (ε) = 314 nm (3700), 420 nm (3900), 487 nm (6800), 735 nm (1100), MS (MALDI-MS-MS, 68 eV; m/z (%)), 839.7 ([(Cp′Ni)$_2$Te$_2$ − H]$^+$, 100), 527.2 ([(Cp′Ni)$_2$Te$_2$ − iPr − Ni]$^+$, 80). Anal. (Cp′Ni)$_2$Te$_2{\cdot}$0.25THF (Calcd C, 49.03%; H, 7.05%. Found C, 49.07%; H, 7.04%).

Synthesis of (Cp′$_2$Ni)$^+$BF$_4$ (4). A solution of (Cp′NiS)$_2$ (214 mg, 0.33 mmol) in 10 mL of dichloromethane was added to a CH_2Cl_2 solution of $FcBF_4$ (81 mg, 0.30 mmol) over 5 min at room temperature, yielding a clear black solution, which was stirred overnight. The solvent was then removed under vacuum, and the resulting dark red solid was washed with 5 × 5 mL of pentane and then with portions of 20 mL of toluene, until the wash became colorless. The red solid was then extracted with 20 mL of dichloromethane. The mixture was filtered, and the filtrate was collected and evaporated to dryness. A small amount of dark red block crystals were collected (yield, 30%). $C_{34}H_{58}NiBF_4$ (MALDI-MS, 66 eV; m/z (%)), 436.8 ($C_{34}H_{58}Ni^+$). ^{1}H NMR (CD_2Cl_2, 300 MHz, ppm) δ 13.96 (br, 14H, $CHMe_2$), 8.99 (br, 14H, $CHMe_2$), 3.24 (br, 28H, $CHMe_2$). Anal. (Cp′$_2$Ni)$^+$BF$_4$ (Calcd C, 66.69%; H, 9.55%. Found C, 66.87%; H, 9.35%).

■ ASSOCIATED CONTENT

Ⓢ Supporting Information

Figures S1−S14. This material is available free of charge via the Internet at http://pubs.acs.org.

■ AUTHOR INFORMATION

Corresponding Author

*berry@chem.wisc.edu

Notes

The authors declare no competing financial interest.

■ ACKNOWLEDGMENTS

We thank the National Science Foundation for support under CHE-1041748 and CHE-1300464. S.D. thanks Cornell University, the Alfred P. Sloan Foundation, and the Max-Planck Society for support. Portions of this research were carried out at the Stanford Synchrotron Radiation Lightsource, a national user facility operated by Stanford University on behalf of the DOE, BES. The SSRL SMB Program is supported by DOE, BER, and NIH, NCRR, BMTP. A.W.G. acknowledges support by a TRO grant of the University of California San Diego the Department of Energy, Biological and Environmental Research (DE-AC36-99G0-10337) and computational time via NSF XSEDE awards TG-MCB090110 and TGCHE130010. This work used the Extreme Science and Engineering Discovery Environment (XSEDE), which is supported by National Science Foundation grant number ACI-1053575. K.M.L. thanks the Cornell University College of Arts and Sciences for startup funding. Additionally, we thank Dr. Jixin Cheng for assistance with XPS data collection, Prof. Daniel Fredrickson and Amelia B. Hadler for help with the synthesis of Na_2Te_2, Brian Dolinar for crystallographic assistance, and Thomas Brunold and Larry Dahl for helpful advice.

■ REFERENCES

(1) (a) Agar, J. N.; Krebs, C.; Frazzon, J.; Huynh, B. H.; Dean, D. R.; Johnson, M. K. *Biochemistry* **2000**, *39*, 7856. (b) Mattoussi, H.; Mauro, J. M.; Goldman, E. R.; Anderson, G. P.; Sundar, V. C.; Mikulec, F. V.; Bawendi, M. G. *J. Am. Chem. Soc.* **2000**, *122*, 12142. (c) Park, J.-H.; Dorrestein, P. C.; Zhai, H.; Kinsland, C.; McLafferty, F. W.; Begley, T. P. *Biochemistry* **2003**, *42*, 12430. (d) Yuvaniyama, P.; Agar, J. N.; Cash, V. L.; Johnson, M. K.; Dean, D. R. *Proc. Natl. Acad. Sci. U. S. A.* **2000**, *97*, 599. (e) Nuttall, K. L. *Med. Hypotheses* **1987**, *24*, 217. (f) Ye, L.; Yong, K.-T.; Liu, L.; Roy, I.; Hu, R.; Zhu, J.; Cai, H.; Law, W.-C.; Liu, J.; Wang, K.; Liu, J.; Liu, Y.; Hu, Y.; Zhang, X.; Swihart, M. T.; Prasad, P. N. *Nat. Nanotechnol.* **2012**, *7*, 453. (g) Pearce, C. I.; Pattrick, R. A. D.; Law, N.; Charnock, J. M.; Coker, V. S.; Fellowes, J. W.; Oremland, R. S.; Lloyd, J. R. *Environ. Technol.* **2009**, *30*, 1313.

(2) (a) Borg, O.; Hammer, N.; Enger, B. C.; Myrstad, R.; Lindvag, O. A.; Eri, S.; Skagseth, T. H.; Rytter, E. *J. Catal.* **2011**, *279*, 163. (b) Hansen, L. P.; Ramasse, Q. M.; Kisielowski, C.; Brorson, M.; Johnson, E.; Topsoe, H.; Helveg, S. *Angew. Chem., Int. Ed.* **2011**, *50*, 10153. (c) Pashigreva, A. V.; Klimov, O. V.; Bukhtiyarova, G. A.; Kochubey, D. I.; Prosvirin, I. P.; Chesalov, Y. A.; Zaikovskii, V. I.; Noskov, A. S. *Catal. Today* **2010**, *150*, 164. (d) Halbert, T. R.; McGauley, K.; Pan, W. H.; Czernuszewicz, R. S.; Stiefel, E. I. *J. Am. Chem. Soc.* **1984**, *106*, 1849. (e) Meneses, A. B.; Antonello, S.; Arevalo, M. C.; Gonzalez, C. C.; Sharma, J.; Wallette, A. N.; Workentin, M. S.; Maran, F. *Chem.—Eur. J.* **2007**, *13*, 7983. (f) Sweeney, Z. K.; Polse, J. L.; Bergman, R. G.; Andersen, R. A. *Organometallics* **1999**, *18*, 5502. (g) Bergwerff, J. A.; Jansen, M.; Leliveld, B. G.; Visser, T.; de Jong, K. P.; Weckhuysen, B. M. *J. Catal.* **2006**, *243*, 292. (h) Karunadasa, H. I.; Montalvo, E.; Sun, Y.; Majda, M.; Long, J. R.; Chang, C. J. *Science* **2012**, *335*, 698. (i) Kim, M. S.; Rodriguez, N. M.; Baker, R. T. K. *J. Catal.* **1993**, *143*, 449. (j) Lecrenay, E.; Sakanishi, K.; Mochida, I. *Catal. Today* **1997**, *39*, 13. (k) Raybaud, P.; Hafner, J.; Kresse, G.; Kasztelan, S.; Toulhoat, H. *J. Catal.* **2000**, *189*, 129. (l) Wang, X.; Wang, X.; Guo, H.; Wang, Z.; Ding, K. *Chem.—Eur. J.* **2005**, *11*, 4078. (m) Vrinat, M.; Lacroix, M.; Breysse, M.; Mosoni, L.; Roubin, M. *Catal. Lett.* **1989**, *3*, 405. (n) Alonso-Vante, N.; Schubert, B.; Tributsch, H. *Mater. Chem. Phys.* **1989**, *22*, 281. (o) Somasundaram, S.; Chenthamarakshan, C. R.; de Tacconi, N. R.; Ming, Y.; Rajeshwar, K. *Chem. Mater.* **2004**, *16*, 3846. (p) Fischer, C.; Alonso-Vante, N.; Fiechter, S.; Tributsch, H. *J. Appl. Electrochem.* **1995**, *25*, 1004.

(3) (a) Kadlag, K. P.; Rao, M. J.; Nag, A. *J. Phys. Chem. Lett.* **2013**, *4*, 1676. (b) Leventis, H. C.; King, S. P.; Sudlow, A.; Hill, M. S.; Molloy, K. C.; Haque, S. A. *Nano Lett.* **2010**, *10*, 1253. (c) Osakada, K.;

DOI: 10.1021/ja511607j
J. Am. Chem. Soc. 2015, 137, 4993−5011

Taniguchi, A.; Kubota, E.; Dev, S.; Tanaka, K.; Kubota, K.; Yamamoto, T. *Chem. Mater.* **1992**, *4*, 562. (d) Chivers, T.; Ritch, J. S.; Robertson, S. D.; Konu, J.; Tuononen, H. M. *Acc. Chem. Res.* **2010**, *43*, 1053. (e) Rao, D. N. R.; Symons, M. C. R.; Wren, B. W. *J. Chem. Soc., Perkin Trans.* **1984**, 1681.

(4) (a) Jeong, S.; Yoo, D.; Jang, J.-t.; Kim, M.; Cheon, J. *J. Am. Chem. Soc.* **2012**, *134*, 18233. (b) Lai, C.-H.; Lu, M.-Y.; Chen, L.-J. *J. Mater. Chem.* **2012**, *22*, 19. (c) Li, B.; Xie, Y.; Xue, Y. *J. Phys. Chem. C* **2007**, *111*, 12181. (d) Slocik, J. M.; Moore, J. T.; Wright, D. W. *Nano Lett.* **2002**, *2*, 169. (e) Zhang, F.; Wong, S. S. *Chem. Mater.* **2009**, *21*, 4541. (f) Noh, J.; Murase, T.; Nakajima, K.; Lee, H.; Hara, M. *J. Phys. Chem. B* **2000**, *104*, 7411.

(5) (a) Alberola, A.; Llusar, R.; Triguero, S.; Vicent, C.; Sokolov, M. N.; Gomez-Garcia, C. *J. Mater. Chem.* **2007**, *17*, 3440. (b) Nagata, K.; Naruta, Y.; Yakiyama, M.; Narita, Y.; Yakeyama, M.; Osada, K. Polyacene compound for organic semiconductor thin film used for organic semiconductor element and transistor, has specific structure. WO2005080304-A1, 2005. (c) Ho, W.; Yu, J. C.; Lin, J.; Yu, J.; Li, P. *Langmuir* **2004**, *20*, 5865. (d) Joo, J.; Na, H. B.; Yu, T.; Yu, J. H.; Kim, Y. W.; Wu, F.; Zhang, J. Z.; Hyeon, T. *J. Am. Chem. Soc.* **2003**, *125*, 11100. (e) Sun, Z.; Yang, Z.; Zhou, J.; Yeung, M. H.; Ni, W.; Wu, H.; Wang, J. *Angew. Chem., Int. Ed.* **2009**, *48*, 2881. (f) Vogel, R.; Hoyer, P.; Weller, H. *J. Phys. Chem.* **1994**, *98*, 3183. (g) Li, J.; Liszewski, Y. Y.; MacAdams, L. A.; Chen, F.; Mulley, S.; Proserpio, D. M. *Chem. Mater.* **1996**, *8*, 598. (h) Mitzi, D. B.; Copel, M.; Murray, C. E. *Adv. Mater.* **2006**, *18*, 2448. (i) Ritch, J. S.; Chivers, T.; Afzaal, M.; O'Brien, P. *Chem. Soc. Rev.* **2007**, *36*, 1622. (j) Tablero, C. *Sol. Energy Mater. Sol. Cells* **2006**, *90*, 588.

(6) (a) Antonello, S.; Daasbjerg, K.; Jensen, H.; Taddei, F.; Maran, F. *J. Am. Chem. Soc.* **2003**, *125*, 14905. (b) Hoffman, M. Z.; Hayon, E. *J. Am. Chem. Soc.* **1972**, *94*, 7950. (c) Modelli, A.; Jones, D. *J. Phys. Chem. A* **2006**, *110*, 10219. (d) Carles, S.; Lecomte, F.; Schermann, J. P.; Desfrançois, C.; Xu, S.; Nilles, J. M.; Bowen, K. H.; Bergès, J.; Houée-Levin, C. *J. Phys. Chem. A* **2001**, *105*, 5622. (e) Wenska, G.; Filipiak, P.; Asmus, K.-D.; Bobrowski, K.; Koput, J.; Marciniak, B. *J. Phys. Chem. B* **2008**, *112*, 10045. (f) Gauduel, Y.; Marignier, J. L.; Belloni, J.; Gelabert, H. *J. Phys. Chem. A* **1997**, *101*, 8979. (g) Cremonini, M. A.; Lunazzi, L.; Placucci, G. *J. Org. Chem.* **1993**, *58*, 3805. (h) Tung, T.-L.; Stone, J. A. *Can. J. Chem.* **1975**, *53*, 3153. (i) Klein, D. L.; Roth, R.; Lim, A. K. L.; Alivisatos, A. P.; McEuen, P. L. *Nature* **1997**, *389*, 699.

(7) (a) Asmus, K. D. *Acc. Chem. Res.* **1979**, *12*, 436. (b) Musker, W. K. *Acc. Chem. Res.* **1980**, *13*, 200. (c) Zhang, S.; Wang, S.; Su, Y.; Qiu, Y.; Zhang, Z.; Wang, X. *Nat. Commun.* **2014**, *5*, 4127. (d) Zhang, S.; Wang, X.; Sui, Y.; Wang, X. *J. Am. Chem. Soc.* **2014**, *136*, 14666.

(8) Berry, J. F. *Chem.—Eur. J.* **2010**, *16*, 2719.

(9) Pyykko, P.; Atsumi, M. *Chem.—Eur. J.* **2009**, *15*, 186.

(10) Alvarez, S. *Dalton Trans.* **2013**, *42*, 8617.

(11) (a) Terzis, A.; Rivest, R. *Inorg. Chem.* **1973**, *12*, 2132. (b) Elder, R. C.; Trkula, M. *Inorg. Chem.* **1977**, *16*, 1048. (c) York, J. T.; Brown, E. C.; Tolman, W. B. *Angew. Chem., Int. Ed.* **2005**, *44*, 7745.

(12) Yao, S.; Milsmann, C.; Bill, E.; Wieghardt, K.; Driess, M. *J. Am. Chem. Soc.* **2008**, *130*, 13536.

(13) (a) Franke, S. M.; Heinemann, F. W.; Meyer, K. *Chem. Sci.* **2014**, *5*, 942. (b) Camp, C.; Antunes, M. A.; Garcia, G.; Ciofini, I.; Santos, I. C.; Pecaut, J.; Almeida, M.; Marcalo, J.; Mazzanti, M. *Chem. Sci.* **2014**, *5*, 841.

(14) Yao, S. L.; Xiong, Y.; Zhang, X. H.; Schlangen, M.; Schwarz, H.; Milsmann, C.; Driess, M. *Angew. Chem., Int. Ed.* **2009**, *48*, 4551.

(15) Yao, S. A.; Lancaster, K. M.; Gotz, A. W.; DeBeer, S.; Berry, J. F. *Chem.—Eur. J.* **2012**, *18*, 9179.

(16) Brown, E. C.; York, J. T.; Antholine, W. E.; Ruiz, E.; Alvarez, S.; Tolman, W. B. *J. Am. Chem. Soc.* **2005**, *127*, 13752.

(17) Alvarez, S.; Hoffmann, R.; Mealli, C. *Chem.—Eur. J.* **2009**, *15*, 8358.

(18) Neese, F. *J. Phys. Chem. Solids* **2004**, *65*, 781.

(19) Sarangi, R.; Yang, L.; Winikoff, S. G.; Gagliardi, L.; Cramer, C. J.; Tolman, W. B.; Solomon, E. I. *J. Am. Chem. Soc.* **2011**, *133*, 17180.

(20) (a) Ponec, R.; Ramos-Cordoba, E.; Salvador, P. *J. Phys. Chem. A* **2013**, *117*, 1975. (b) Vidossich, P.; Lledos, A. *Dalton Trans.* **2014**, 11145.

(21) Yao, S.; Hrobárik, P.; Meier, F.; Rudolph, R.; Bill, E.; Irran, E.; Kaupp, M.; Driess, M. *Chem.—Eur. J.* **2013**, *19*, 1246.

(22) (a) Sitzmann, H.; Saurenz, D.; Wolmershauser, G.; Klein, A.; Boese, R. *Organometallics* **2001**, *20*, 700. (b) Schär, M.; Saurenz, D.; Zimmer, F.; Schädlich, I.; Wolmershäuser, G.; Demeshko, S.; Meyer, F.; Sitzmann, H.; Heigl, O. M.; Köhler, F. H. *Organometallics* **2013**, *32*, 6298.

(23) Yao, S. A.; Corcos, A. R.; Infante, I.; Hillard, E. A.; Clerac, R. *J. Am. Chem. Soc.* **2014**, *136*, 13538.

(24) Similar results have been found upon oxidation of **1**. Crystal data: $C_{51}H_{81}Ni_3S_4BF_4$, FW = 1091.39; hexagonal, a = 13.518(1) Å, c = 50.616(1) Å, V = 8010.4(4) Å^3, Z = 6. R1 = 0.0588, wR2 = 0.1234; S−S distance = 2.051(1) Å, 2.075(1) Å.

(25) (a) Song, L. C.; Cheng, H. W.; Chen, X.; Hu, Q. M. *Eur. J. Inorg. Chem.* **2004**, 3147. (b) Shin, J. H.; Savage, W.; Murphy, V. J.; Bonanno, J. B.; Churchill, D. G.; Parkin, G. *J. Chem. Soc., Dalton Trans.* **2001**, 1732.

(26) Song, L. C.; Cheng, H. W.; Hu, Q. M. *J. Organomet. Chem.* **2004**, *689*, 1849.

(27) (a) Lesch, D. A.; Rauchfuss, T. B. *Inorg. Chem.* **1981**, *20*, 3583. (b) Lesch, D. A.; Rauchfuss, T. B. *Inorg. Chem.* **1983**, *22*, 1854. (c) McConnachie, J. M.; Ansari, M. A.; Ibers, J. A. *Inorg. Chim. Acta* **1992**, *198*, 85. (d) Kato, S.; Niyomura, O.; Kawahara, Y.; Kanda, T. *J. Chem. Soc., Dalton Trans.* **1999**, 1677. (e) Robertson, S. D.; Chivers, T. *Dalton Trans.* **2008**, 1765.

(28) (a) Berry, J. F.; Bill, E.; Bothe, E.; George, S. D.; Mienert, B.; Neese, F.; Wieghardt, K. *Science* **2006**, *312*, 1937. (b) Kornecki, K. P.; Briones, J. F.; Boyarskikh, V.; Fullilove, F.; Autschbach, J.; Schrote, K. E.; Lancaster, K. M.; Davies, H. M. L.; Berry, J. F. *Science* **2013**, *342*, 351. (c) DeBeer, S.; Neese, F. *Inorg. Chem.* **2010**, *49*, 1849. (d) DeBeer, S.; Sarangi, R.; Rudd, D. J.; Szilagyi, R. K.; Ribas, X.; Rovira, C.; Almeida, M.; Hodgson, K. O.; Hedman, B.; Solomon, E. I. *J. Am. Chem. Soc.* **2007**, *129*, 2316. (e) Lancaster, K. M.; Roemelt, M.; Ettenhuber, P.; Hu, Y.; Ribbe, M. W.; Neese, F.; Bergmann, U.; DeBeer, S. *Science* **2011**, *334*, 974. (f) Ray, K.; Petrenko, T.; Wieghardt, K.; Neese, F. *J. Chem. Soc., Dalton Trans.* **2007**, 1552.

(29) (a) Solomon, E. I.; Hedman, B.; Hodgson, K. O.; Dey, A.; Szilagyi, R. K. *Coord. Chem. Rev.* **2005**, *249*, 97. (b) Sarangi, R.; York, J. T.; Helton, M. E.; Fujisawa, K.; Karlin, K. D.; Tolman, W. B.; Hodgson, K. O.; Hedman, B.; Solomon, E. I. *J. Am. Chem. Soc.* **2007**, *130*, 676.

(30) Martin-Diaconescu, V.; Kennepohl, P. *J. Am. Chem. Soc.* **2007**, *129*, 3034.

(31) Colpas, G. J.; Maroney, M. J.; Bagyinka, C.; Kumar, M.; Willis, W. S.; Suib, S. L.; Mascharak, P. K.; Baidya, N. *Inorg. Chem.* **1991**, *30*, 920.

(32) Kau, L. S.; Spira-Solomon, D. J.; Penner-Hahn, J. E.; Hodgson, K. O.; Solomon, E. I. *J. Am. Chem. Soc.* **1987**, *109*, 6433.

(33) We note, however, that due to challenges in unambiguously assigning the transitions superimposed on the Ni K-edge, the changes are difficult to quantitatively assess and these conclusions can only be drawn taking into account both the Ni and the S K-edge data.

(34) Sarangi, R.; George, S. D.; Rudd, D. J.; Szilagyi, R. K.; Ribas, X.; Rovira, C.; Almeida, M.; Hodgson, K. O.; Hedman, B.; Solomon, E. I. *J. Am. Chem. Soc.* **2007**, *129*, 2316.

(35) Moulder, J. F.; Stickle, W. F.; Sobol, P. E.; Bomben, K. D. *Handbook of X-ray Photoelectron Spectroscopy*; Perkin-Elmer Corporation: Eden Prairie, MN, 1992.

(36) (a) Desrochers, P. J.; Nebesny, K. W.; LaBarre, M. J.; Bruck, M. A.; Neilson, G. F.; Sperline, R. P.; Enemark, J. H.; Backes, G.; Wieghardt, K. *Inorg. Chem.* **1994**, *33*, 15. (b) Nippe, M.; Goodman, S. M.; Fry, C. G.; Berry, J. F. *J. Am. Chem. Soc.* **2011**, *133*, 2856. (c) Feltham, R. D.; Brant, P. *J. Am. Chem. Soc.* **1982**, *104*, 641.

(37) Muller, A.; Jaegermann, W. *Inorg. Chem.* **1979**, *18*, 2631.

(38) Rolfe, J. *J. Chem. Phys.* **1968**, *49*, 4193.

DOI: 10.1021/ja511607j
J. Am. Chem. Soc. 2015, 137, 4993−5011

(39) Yee, K. K.; Rogstad, A.; Barrow, R. F. *J. Chem. Soc., Faraday Trans. 2* **1972**, *68*, 1808.
(40) Mulliken, R. S. *J. Chem. Phys.* **1955**, *23*, 1833.
(41) Guerra, C. F.; Handgraaf, J.-W.; Baerends, E. J.; Bickelhaupt, F. M. *J. Comput. Chem.* **2004**, *25*, 189.
(42) Bader, R. F. W. *Chem. Phys. Lett.* **2009**, *472*, 149.
(43) Williams, V. A.; Hulley, E. B.; Wolczanski, P. T.; Lancaster, K. M.; Lobkovsky, E. B. *Chem. Sci.* **2013**, *4*, 3636.
(44) Dumont, É.; Loos, P.-F.; Assfeld, X. *Chem. Phys. Lett.* **2008**, *458*, 276.
(45) The percent character of the leading configuration increases with the size of the active space. For a (14/12) active space, the leading term is 31%, and for the largest active space explored at the limit of our computational capability, (22/16), this increases to 44%.
(46) Holland, P. L. *Dalton Trans.* **2010**, *39*, 5415.
(47) $C_{51}H_{87}Co_3Se_4$, monoclinic, a = 22.197 Å, b = 13.784 Å, c = 17.207 Å, β = 103.87°, V = 5111.21 Å^3, $C2/c$, Se−Se distances are 2.433 Å.
(48) (a) Scoles, L.; Gambarotta, S. *Inorg. Chim. Acta* **1995**, *235*, 375. (b) Firth, A. V.; Stephan, D. W. *Organometallics* **1997**, *16*, 2183. (c) Hagadorn, J. R.; Arnold, J. *Organometallics* **1998**, *17*, 1355. (d) Firth, A. V.; Witt, E.; Stephan, D. W. *Organometallics* **1998**, *17*, 3716. (e) Guiducci, A. E.; Boyd, C. L.; Mountford, P. *Organometallics* **2006**, *25*, 1167.
(49) (a) Klein, H.-F.; Gass, M.; Koch, U.; Eisenmann, B.; Schafer, H. *Z. Naturforsch., B: J. Chem. Sci.* **1988**, *43*, 830. (b) Pleus, R. J.; Waden, H.; Saak, W.; Haase, D.; Pohl, S. *Dalton Trans.* **1999**, 2601. (c) Iluc, M. V.; Laskowaki, C. A.; Brozek, C. K.; Harrold, N. D.; Hillhouse, G. L. *Inorg. Chem.* **2010**, *49*, 6817.
(50) Yamada, N.; Furukawa, M.; Nishi, M.; Takata, T. *Chem. Lett.* **2002**, *4*, 454.
(51) Thompson, D. P.; Boudjouk, P. *J. Org. Chem.* **1988**, *53*, 2109.
(52) Dehmlow, E. V.; Bollmann, C. *Z. Naturforsch., B: J. Chem. Sci.* **1993**, *48*, 457.
(53) *SMART*; Bruker AXS Inc., Madison, WI, 2007.
(54) Wojdyr, M. *Fityk*; 0.9.3 ed., 2009.
(55) Webb, S. M. *Phys. Scr.* **2005**, *T115*, 1011.
(56) Ravel, B.; Newville, M. *J. Synchrotron Radiat.* **2005**, *12*, 537.
(57) Neese, F.; Becker, U.; Ganyushin, D.; Liakos, D. G.; Kossmann, S.; Petrenko, T.; Riplinger, C.; Wennmohs, F. *ORCA*, 2.8.0 ed.; University of Bonn, Bonn, 2009.
(58) Perdew, J. P.; Yue, W. *Phys. Rev. B* **1986**, *33*, 8800.
(59) Becke, A. D. *J. Chem. Phys.* **1993**, *98*, 1372.
(60) (a) Becke, A. D. *Phys. Rev. A* **1988**, *38*, 3098. (b) Becke, A. D. *J. Chem. Phys.* **1993**, *98*, 5648. (c) Lee, C. T.; Yang, W. T.; Parr, R. G. *Phys. Rev. B* **1988**, *37*, 785.
(61) (a) Bickelhaupt, F. M.; Velde, G. T.; Baerends, E. J.; Guerra, C. F.; Van Gisbergen, S. J. A.; Snijders, J. G.; Ziegler, T. *J. Comput. Chem.* **2001**, *22*, 931. (b) *ADF*; Vrije Universiteit, Amsterdam, The Netherlands, 2010.
(62) Perdew, J. P.; Burke, K.; Ernzerhof, M. *Phys. Rev. Lett.* **1997**, *78*, 1396.
(63) (a) Schreckenbach, G.; Ziegler, T. *J. Phys. Chem. A* **1997**, *101*, 3388. (b) Patchkovskii, S.; Ziegler, T. *J. Chem. Phys.* **1999**, *111*, 5730.
(64) Kafafi, S. A. *J. Phys. Chem. A* **1998**, *102*, 10404.
(65) Schafer, A.; Huber, C.; Ahlrichs, R. *J. Chem. Phys.* **1994**, *100*, 5829.
(66) Flükiger, P.; Lüthi, H. P.; Portmann, S.; Weber, J. *MOLEKEL*, 4.0 ed.; Swiss Center for Scientific Computing: Manno, Switzerland, 2000.
(67) Vanlenthe, E.; Baerends, E. J.; Snijders, J. G. *J. Chem. Phys.* **1993**, *99*, 4597.
(68) Aquilante, F.; Pedersen, T. B.; Veryazov, V.; Lindh, R. *Wiley Interdiscip. Rev.: Comput. Mol. Sci.* **2013**, *3*, 143.

DOI: 10.1021/ja511607j
J. Am. Chem. Soc. 2015, 137, 4993−5011